The Abdus Salam
International Centre for Theoretical Physics

United Nations
Educational, Scientific and
Cultural Organization

IAEA
International Atomic Energy Agency

2332-17

School on Synchrotron and FEL Based Methods and their Multi-Disciplinary Applications

19 - 30 March 2012

Low Density Matter: Scattering and Ultrafast dynamics

Nadia Bingelli

ICTP
Trieste
ITALY

Marc Simon

Laboratoire de Chimie Physique - Martière et Rayonnement
Paris
FRANCE

Low Density Matter : Scattering and Ultrafast dynamics

Marc SIMON

Laboratoire de Chimie Physique-Matière et Rayonnement, Paris 6, France
marc.simon@upmc.fr

Outline

Absorption
Photoionization
Auger effect
Resonant Raman Scattering
Core hole clock spectroscopy
Ultrafast dynamics

Atomic absorption spectra below the ionization threshold

Below the ionization threshold, we consider electronic transitions corresponding to the promotion of one electron of an occupied core orbital to an external empty orbital.

Corehole lifetime

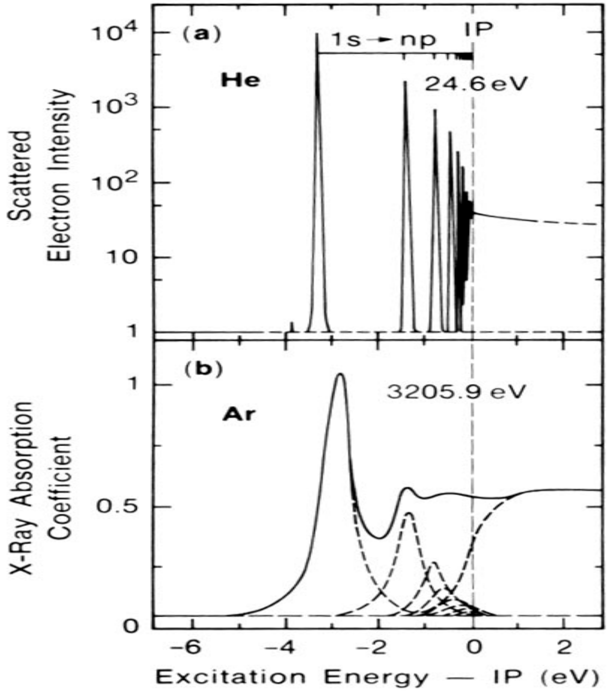

Comparison of the Rydberg serie 1s--> np for helium and argon in gas phase converging toward the Ionization Potential (I.P.) as function of *term values* (excitation energy - IP (eV)).

Inner Shell excitation produces instable intermediate state which decays. The observed resonances in absorption spectra correspond to an excitation from the ground state to an intermediate resonant state. The Full Widh at Half Maximum (FWHM) of the resonance Γ is determined by the core hole lifetime of the intermediate state by the Heisenberg uncertainty principle $\Gamma.\tau$ = h/2π.

$h/2\pi = 6.6 \,.\, 10^{-16}$ eV.s

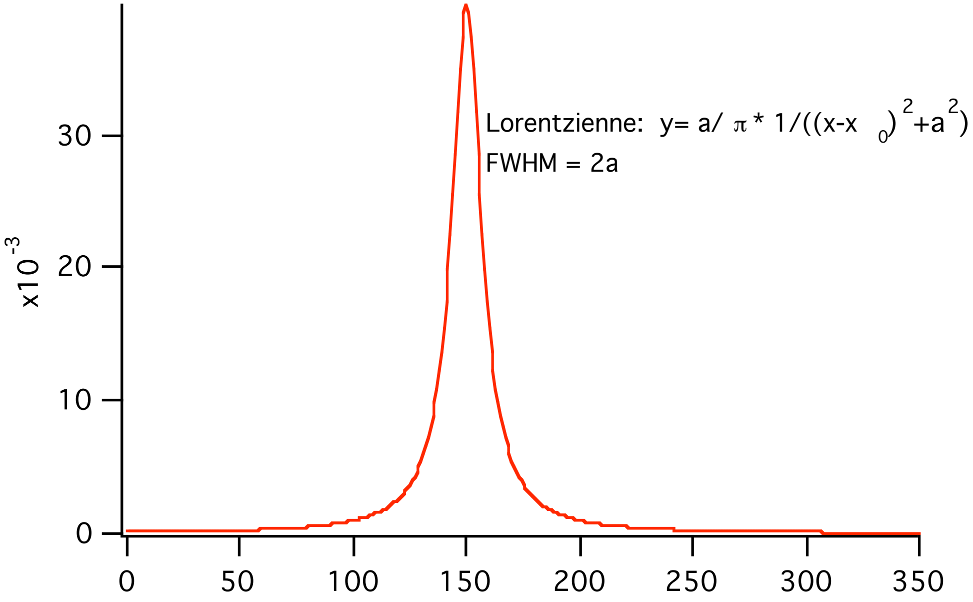

Absorption spectra are systematically broadened by the photon bandwidth (Gaussian) and by the core hole lifetime (Lorentzian). → Voigt profile

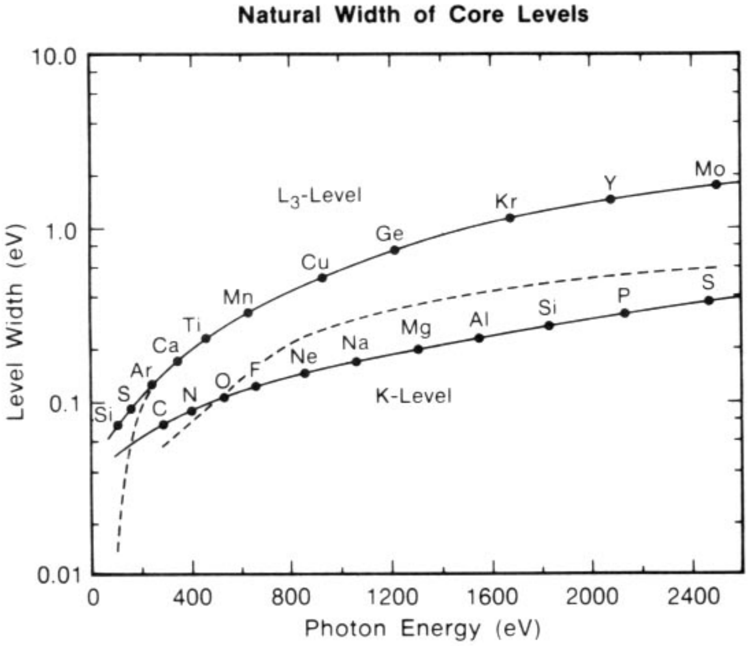

Core hole lifetime broadening of K shells of light elements and for different L3 shells as a function of photon energy.

L3 shell: ionisation of the level $2p^{3/2}$

Molecular Inner Shell resonant excitation

The electron motion are much faster than nuclear motion, electronic and nuclear degrees of freedom can be separated (Born Oppenheimer approximation). The Franck-Condon principle considers that the interatomic distance is constant during the fast excitation process.

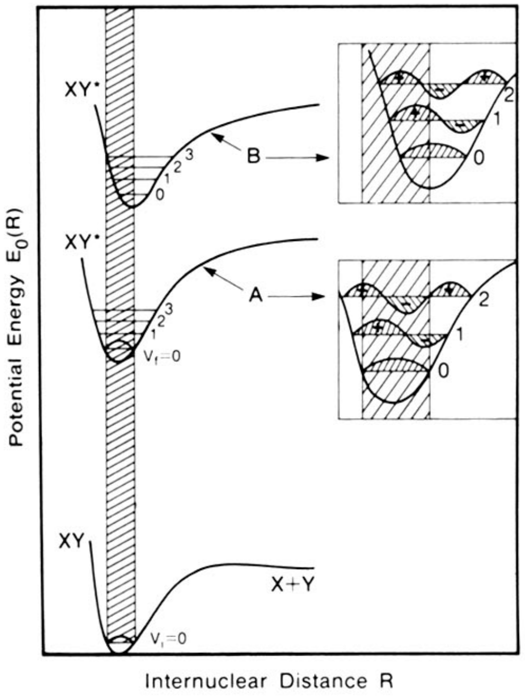

A molecule XY is absorbing a photon. An electronic transition occurs between the ground state and the bound excited state. At the moment of absorption, the excited state is produced in the Franck-Condon region.

2 possibilities:

- A case, the two potentials have their minima at the same internuclear distance. Only the vibration level is $v_f=0$ populated.
- B case, the two potentials do not have their minima at the same internuclear distance. A distribution of vibrational levels is produced according to the Franck-Condon factors.

Core equivalent model

During an electronic transition wich promotes an inner shell electron toward an empty orbital, a localised inner hole is produced and the electronic cloud is adjusted to the new apparent charge of the nucleus. The core equivalent model stipulates that the elctronic cloud is adjusted much faster than the inner shell lifetime.

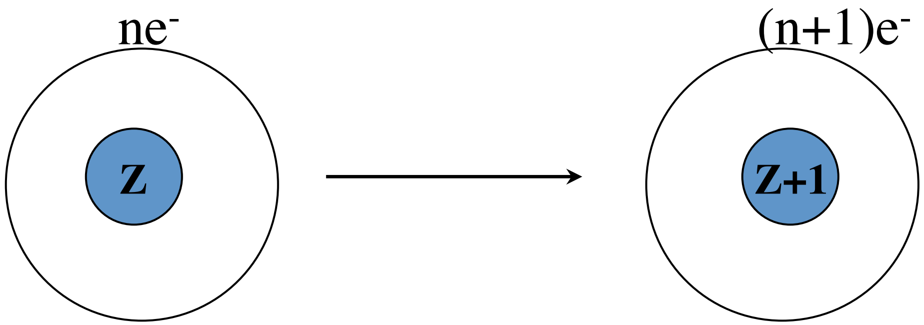

The core excited atom is core equivalent to its successor in the Mendeleiv periodic table.

The core equivalent model allows to predic the geometry of the core excited intermediate state (neutral) as well as Term Values (position of the resonances with respect to the ionization trheshold.).

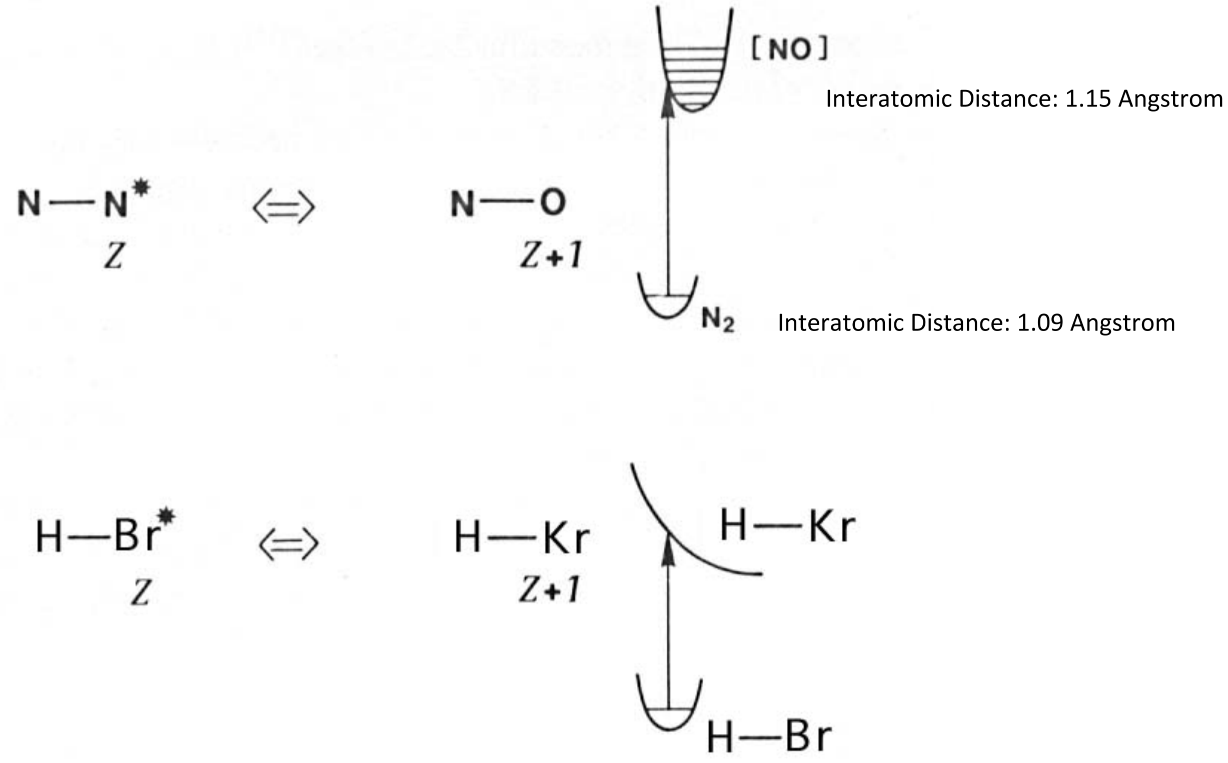

Interatomic Distance: 1.15 Angstrom

Interatomic Distance: 1.09 Angstrom

Examples

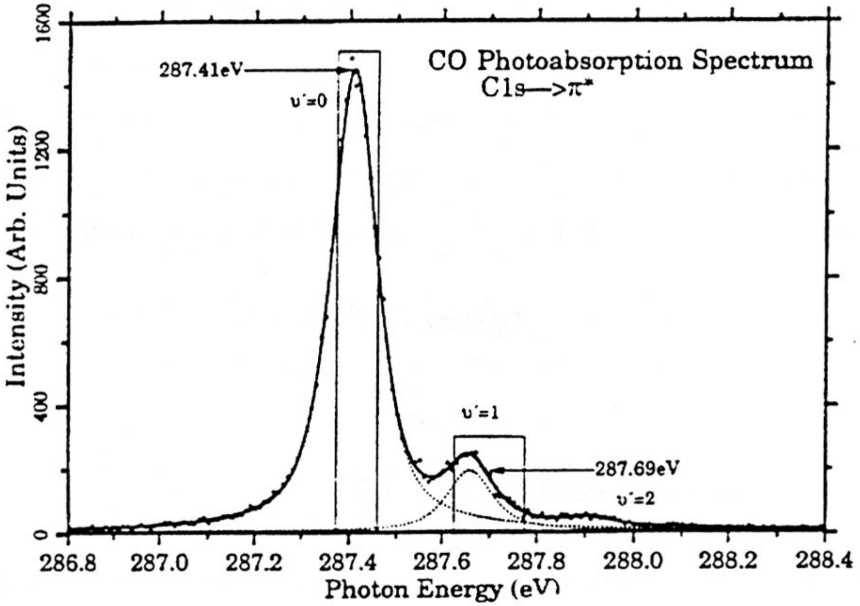

Molecule CO: absorption C_{1s}-->π*
CO d(C,O) = 1.12 Angström
NO d(N,O) = 1.15 Angström

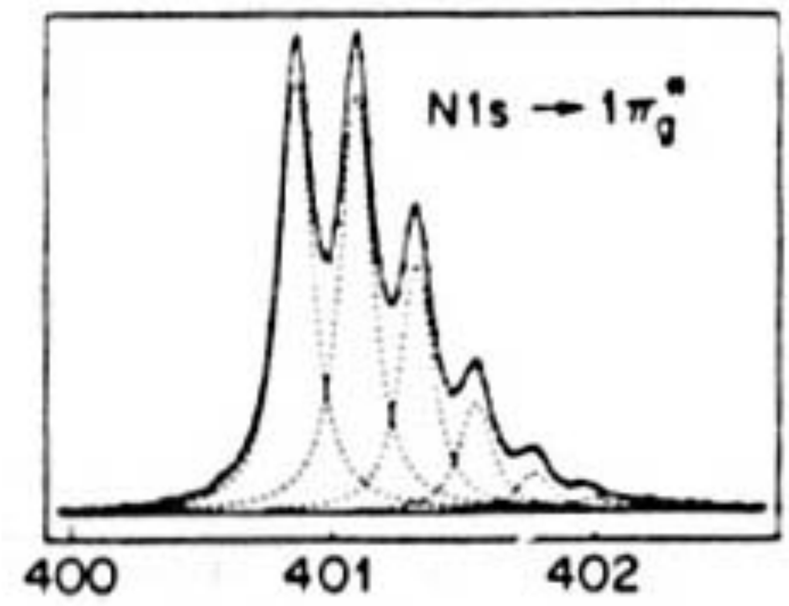

Molecule N_2: absorption N_{1s}-->π*
N_2 d(N,N) = 1.09 Angström
NO d(N,O) = 1.15 Angström

The absorption spectrum is broadened by the core hole lifetime (7 fs).
Vibrational structures are resolved because the energy spacing is superior to the photon bandwidth and the lifetime broadening.

The N_2 absorption spectrum is THE spectrum which determines the performances of the beamline in terms of resolution in the soft x-ray domain.
The figure of merit R is defined as the ratio of the hollow between the two first resonances and the third resonance.

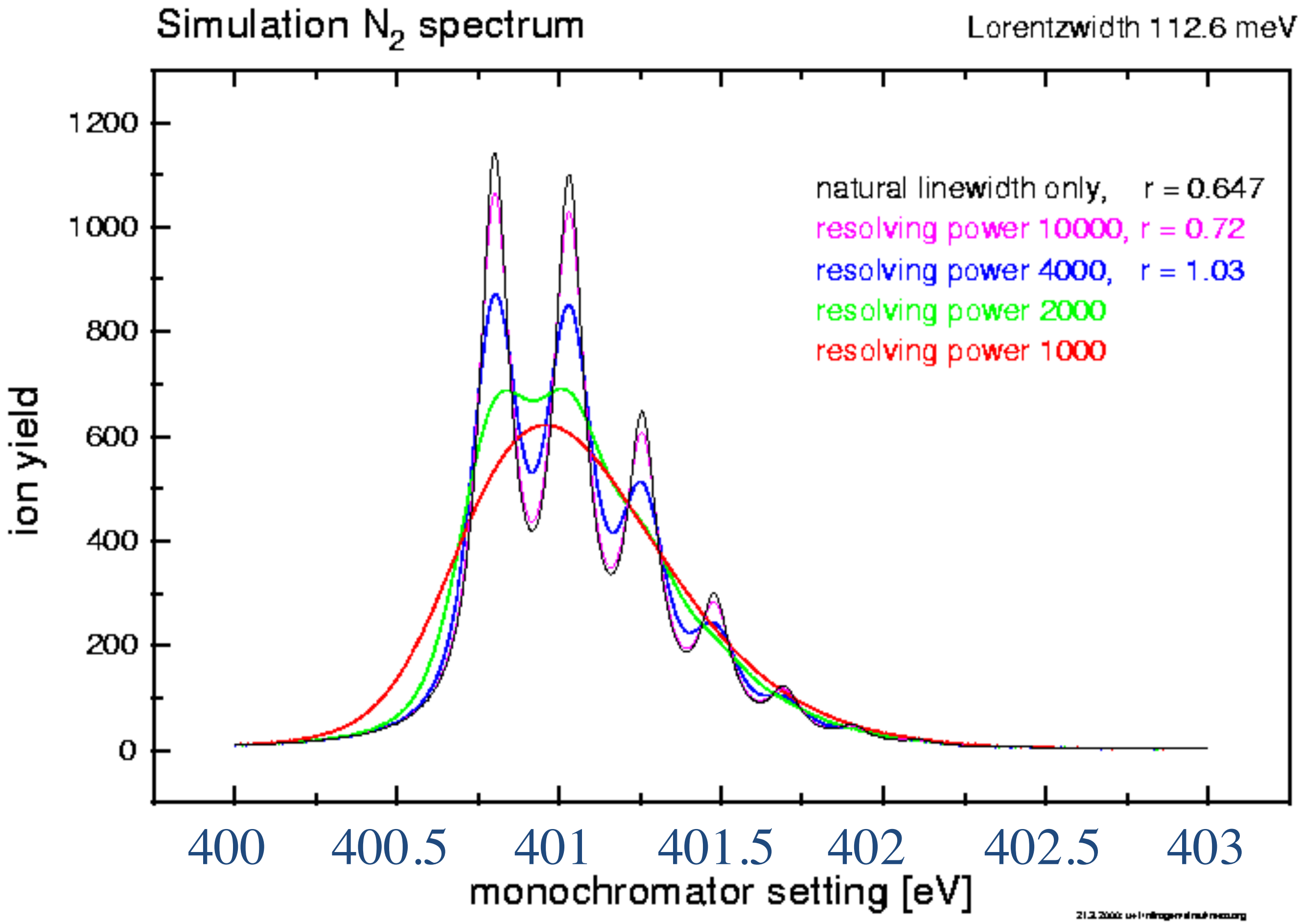

Simulation of nitrogen spectrum with Voigt profiles. Lorentzian line width of 112.6 meV. Gaussian width variing between 40 meV and 400 meV.

http://www-old.bessy.de/~follath/

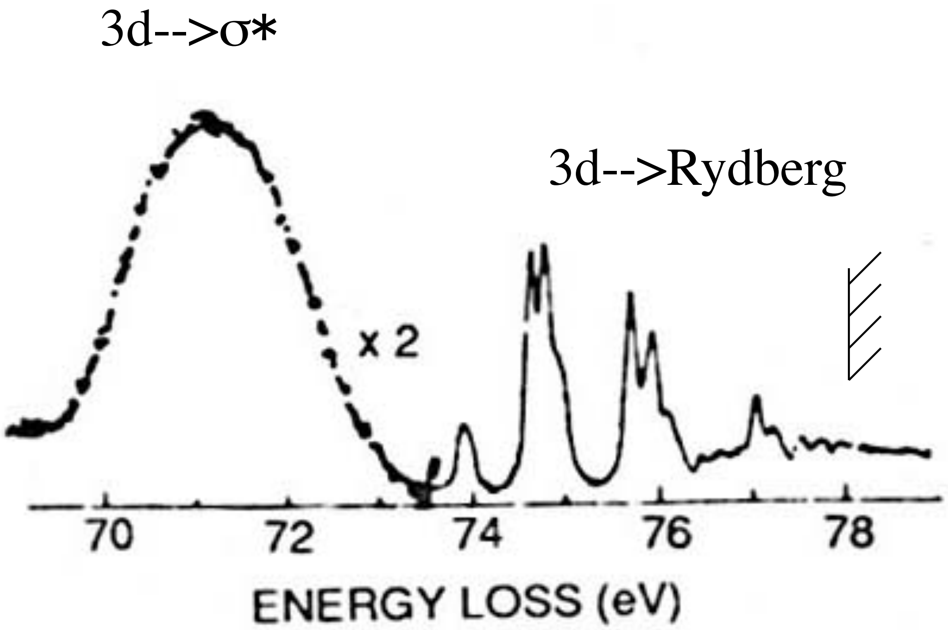

Absorption spectrum of the HBr molecule around the bromine 3d threshold.

Z+1 model: The dissociative character of HKr explains the repulsive character of HBr* after promotion of a 3d electron toward the LUMO σ*, so a very wide resonance is measured.

Example: Absorption spectrum of the BF_3 molecule around the boron 1s.

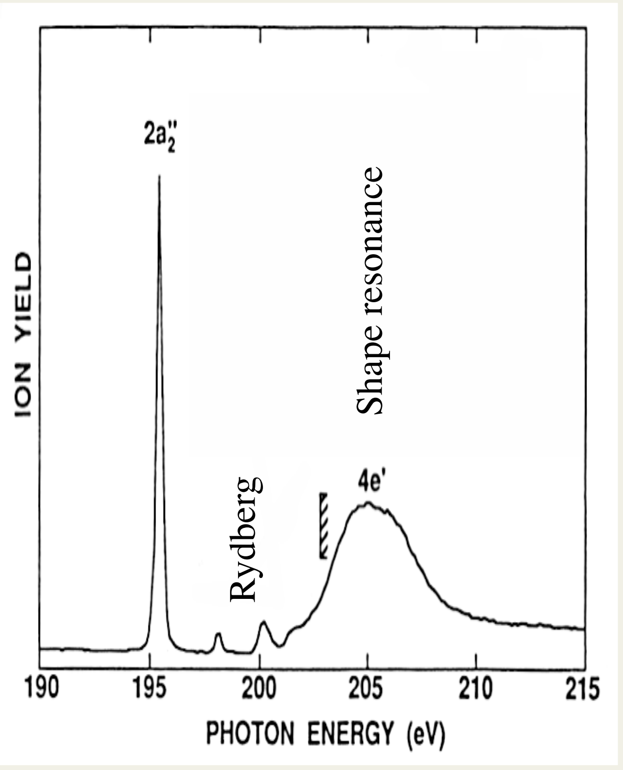

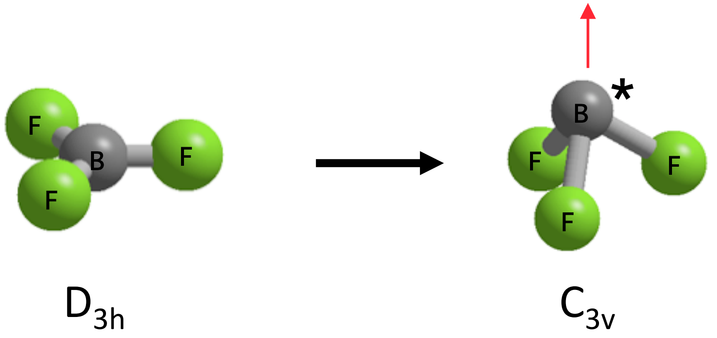

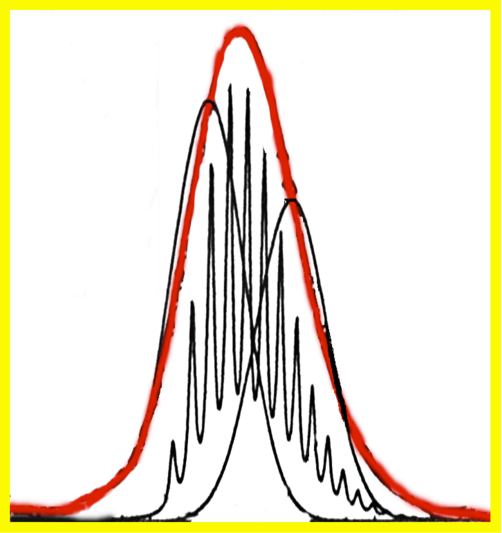

- **Lifetime broadening≈ 64 meV**

- **Vibrational spacing: $\Delta_{vib} \approx$ 63 meV**

- **Resonance FWHM: 350 meV**

Even with an excellent photon bandwidth, it is impossible to resolve vibrational structures due to geometry change plane molecule --> pyramidal molecule.

Photoionization

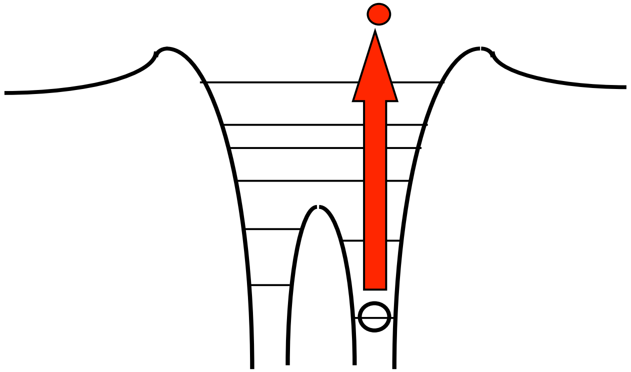

Inner shell photoionization

If the photon energy is high enough, an inner shell electron is ejected into the continuum with a kinetic energy Ec leaving a singly charged molecular ion.

$$\mathbf{Ec = h\nu - Eb} \searrow$$

Binding energy

Inner shell relaxation : the Auger effect

The singly charged ion created after the photoionization process is very instable. Two decay processes are in competition : x-ray fluorescence and Auger effect. The Auger effect dominates in the soft x-ray domain.

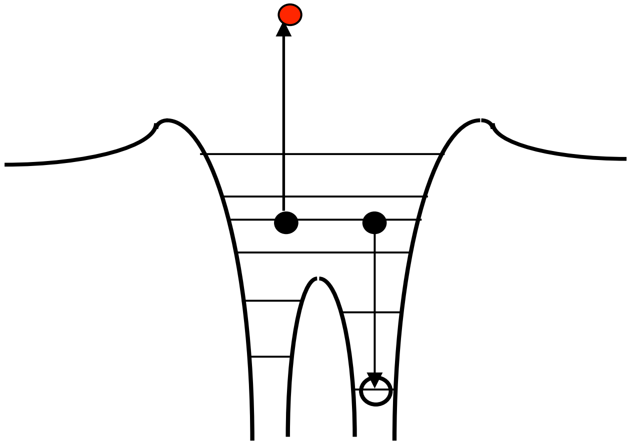

The Auger Effect

Two valence electrons are involved in the Auger effect : one electrons fills the inner shell hole and an other one is ejected into te continuum.

The Auger electron is the one ejected into the continuum. He is leaving a doubly charged ion.

The Auger electron kinetic energy is independent of the photon energy and only dependent on the molecular orbital involved.

Photoionization and Auger relaxation are <u>sequential</u> processes.

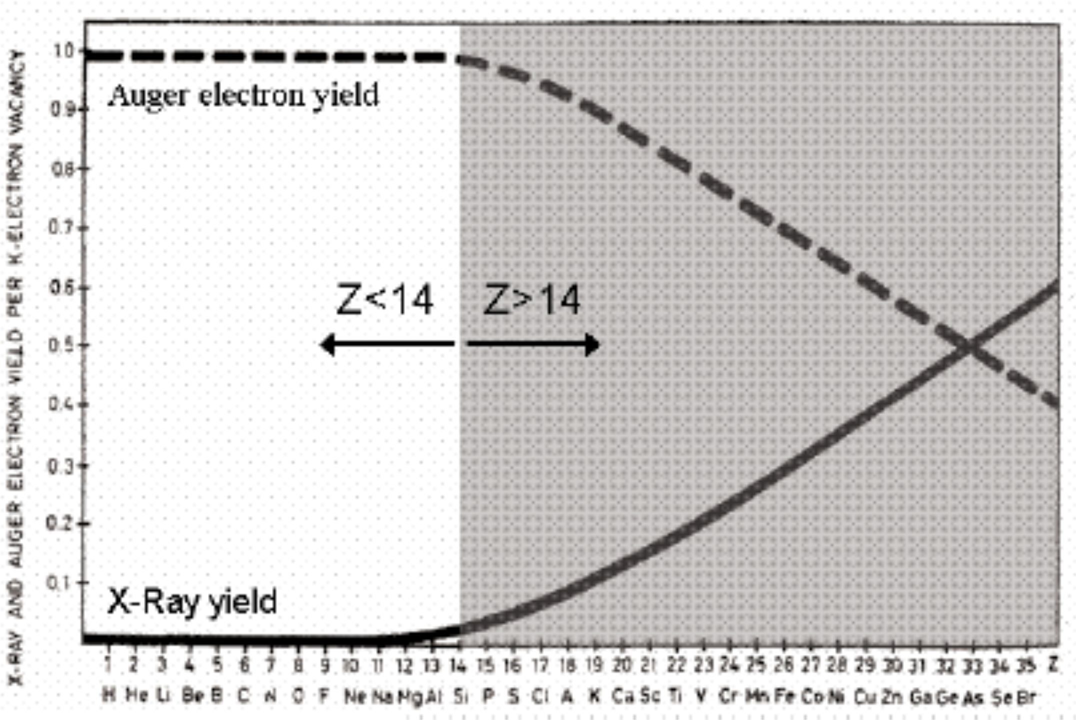

Comparison of Auger and fluorescence yield as a function of the atomic number.

Limit of the model: Post Collision Interaction (P. C. I.)

Close to threshold, the photoelectron is leaving slowly a singly charged ion. The Auger effect occurs when the photoelectron is still close to the ion. After a time close to the core hole lifetime (few femtoseconds), the Auger electron leaves rapidly a doubly charged ion. If the Auger electron escapes faster the coulombic field, then :

- the photoelectron « feels » the field of a doubly charged ion and is decelerated -
- the Auger electron « feels » a singly charged ion and is accelerated.

→ Assymmetric shape

Example: the CO molecule close to carbon 1s threshold

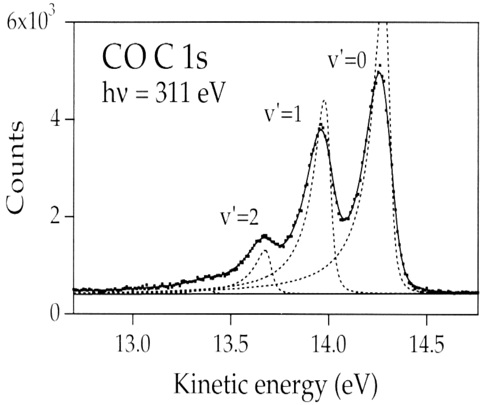

Photoelectron spectrum of the CO molecule measured at 311 eV of photon energy.

Threshold photoelectron without PCI : coincidence between threshold electron and x-ray fluorescence.

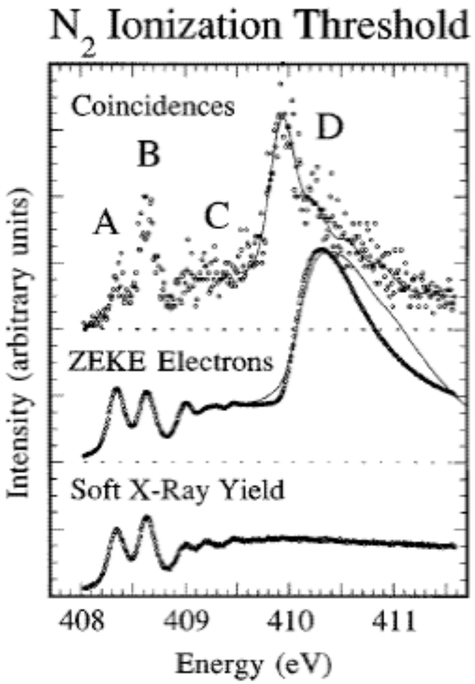

Rubensson et al., PRL 76 (1996) 3919

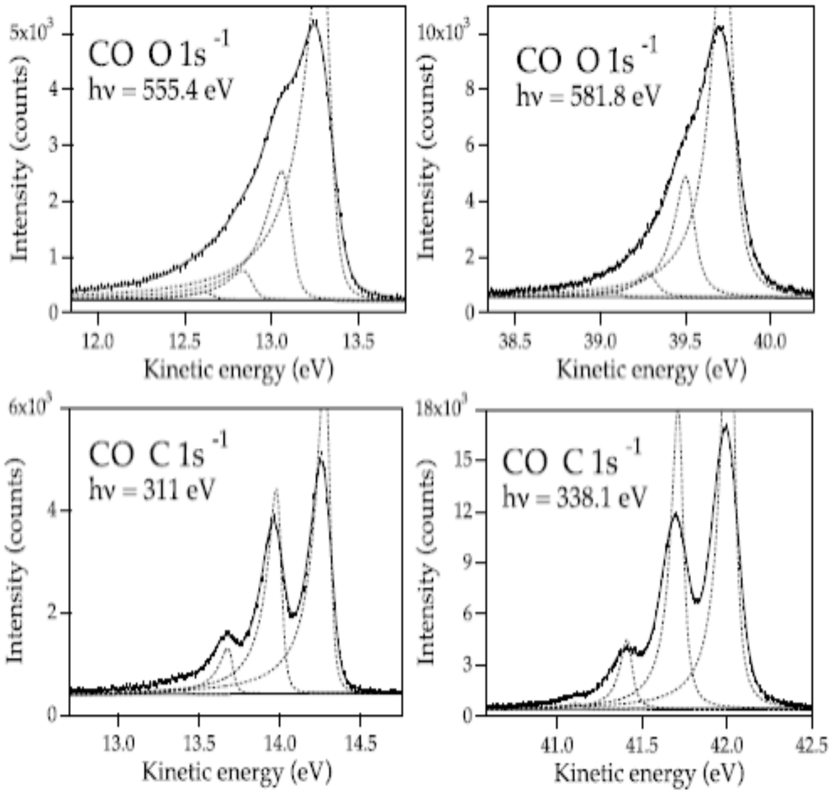

Photoelectron spectra of the CO molecule above the oxygen and carbon 1s.

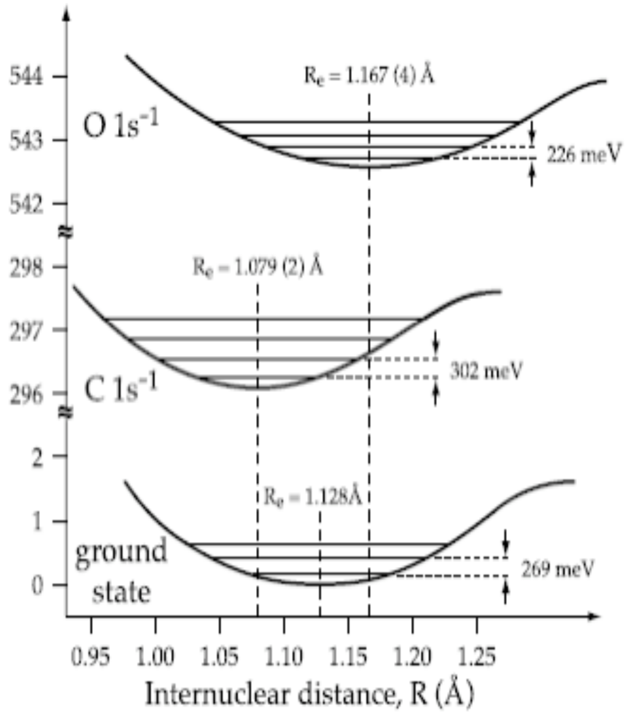

Potential Energy Curves of the CO molecule in the ground state and for the CO^+ ion $C1s^{-1}$ et $O1s^{-1}$.

This shows the antibonding character of the C1s molecular orbital and the bonding character of the O1s molecular orbital.

Kempgens et al. J Phys B 30 L741-L747 (1997)

High resolution: Chemical shift, basis of ESCA
Nobel price in 1981 of K. Siegbahn

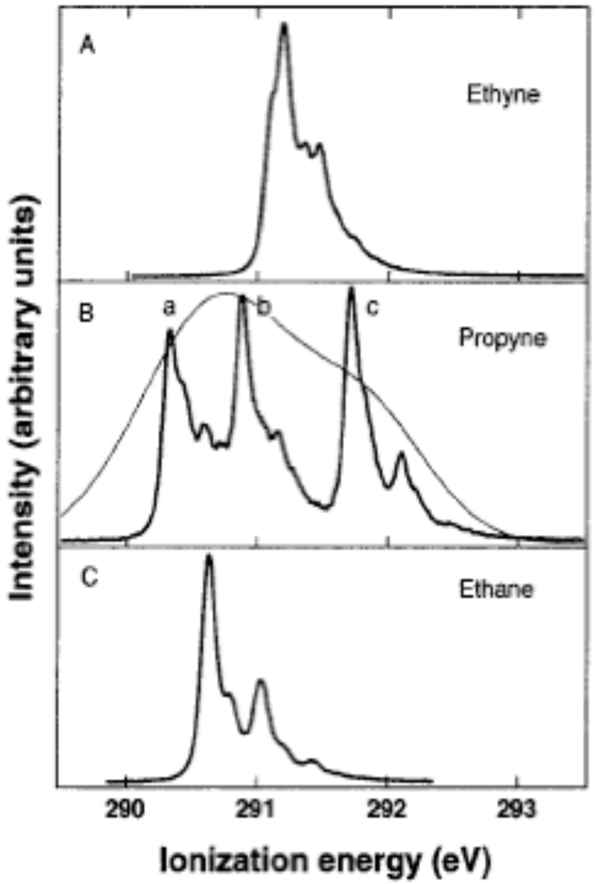

Figure 1. Experimental carbon 1s photoelectron spectra of ethyne, propyne, and ethane. The dotted curve in B shows the previously available data for propyne (ref 3).

Saethre et al., JACS 123 10729-10737 2001

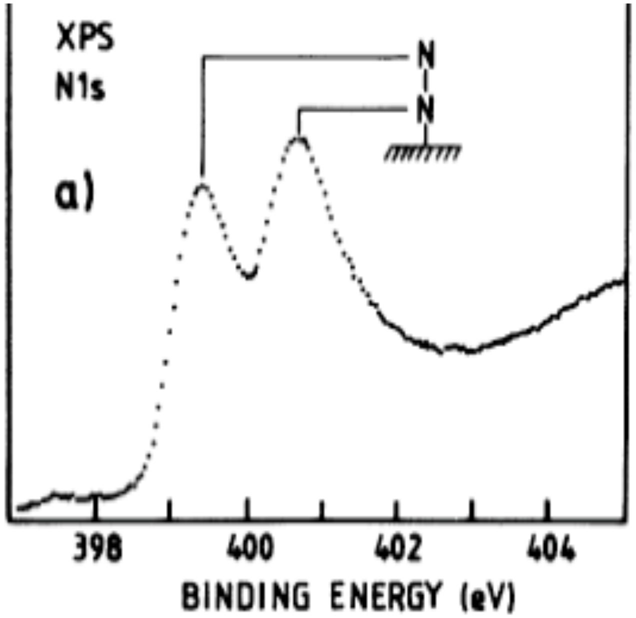

1s Photoemission of nitrogen adsorbed on Ni (100) c(2x2).

Energy shift between C1sσ_g and C1sσ_u orbitals of acethylene

$$\Psi\sigma_g = 1/\sqrt{2}(\Psi_1 + \Psi_2)$$

$$\Psi\sigma_u = 1/\sqrt{2}(\Psi_1 - \Psi_2)$$

For acethylene the CC chemical bond is short (1.2 Angstrom) and the energy shift is 105 meV

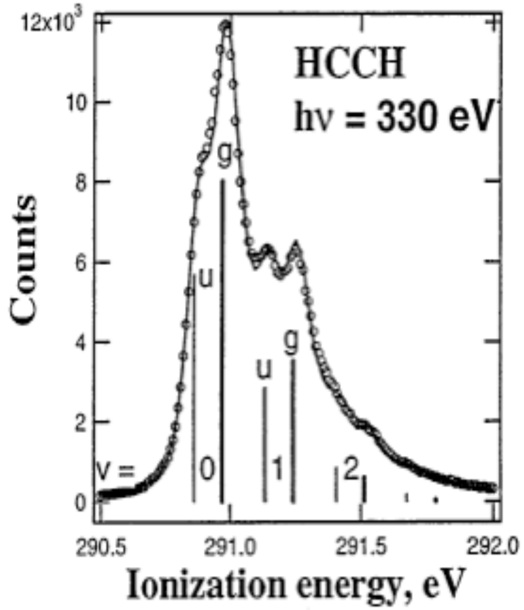

FIG. 1. Carbon 1*s* photoelectron spectrum of HCCH at a photon energy of 330 eV. The points represent the data and the solid curve a fit assuming that carbon-carbon stretching is the only mode contributing to the vibrational structure. The data and the fit extend to both higher and lower energies than shown here. The vertical bars indicate the position and intensity of the different vibrational transitions. The light lines are for $1\sigma_u^{-1}$, and the heavy lines are for $1\sigma_g^{-1}$. The intensities shown for $\upsilon = 2$ and $\upsilon = 3$ contain contributions from CH stretching modes, which were not considered in the fitting procedure.

Thomas et al., Phys. Rev. Lett. 82 (1999) 1120

Auger relaxation

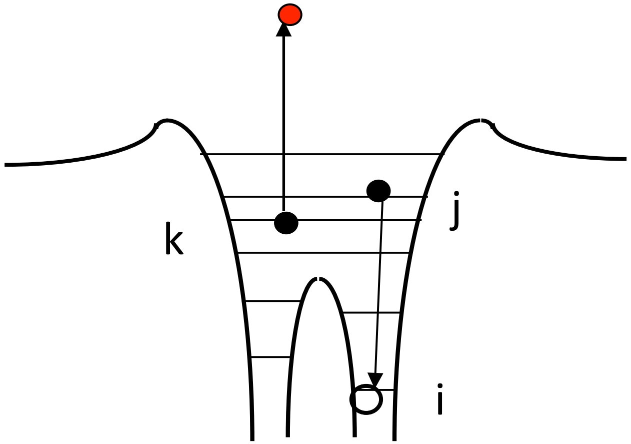

Effet Auger

The Coulomb interaction between the core hole and the valence electrons : the core hole is filled and one electron is ejected into the continuum.

Matrix element:

$$< \underbrace{\varphi_i \chi}_{\text{final}} \left| \frac{1}{r_{12}} \right| \underbrace{\varphi_j \varphi_k}_{\text{initial}} >$$

For molecules: the matrix element is higher when the j and k orbitals are localized close to the core hole i.

⇒ Intra-atomic Auger >> Inter-atomic Auger

Auger electron kinetic energy: $E_A = E_b^i - E_b^{jk}$ $\quad (E_b^{jk} > E_b^j + E_b^k)$

Binding energy of the core hole

Binding energy of the doubly charged ion with the two holes j and k.

⇒ Spectroscopy of doubly charged ions.

Example: Auger spectrum of the NO molecule after oxygen K shell ionization.

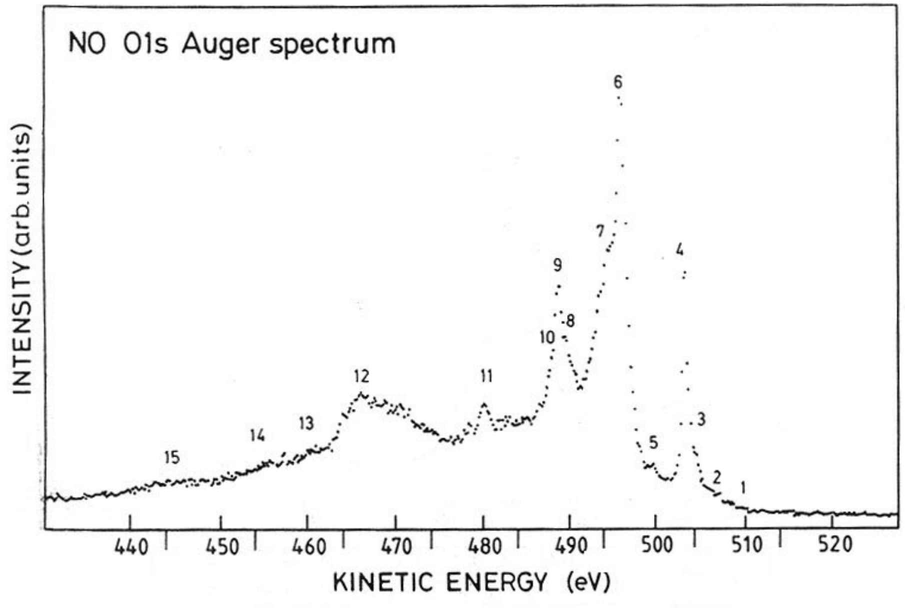

Rq The spectrum is broadened by the lifetime broadening and the analyser resolution but not by the photon bandwidth.

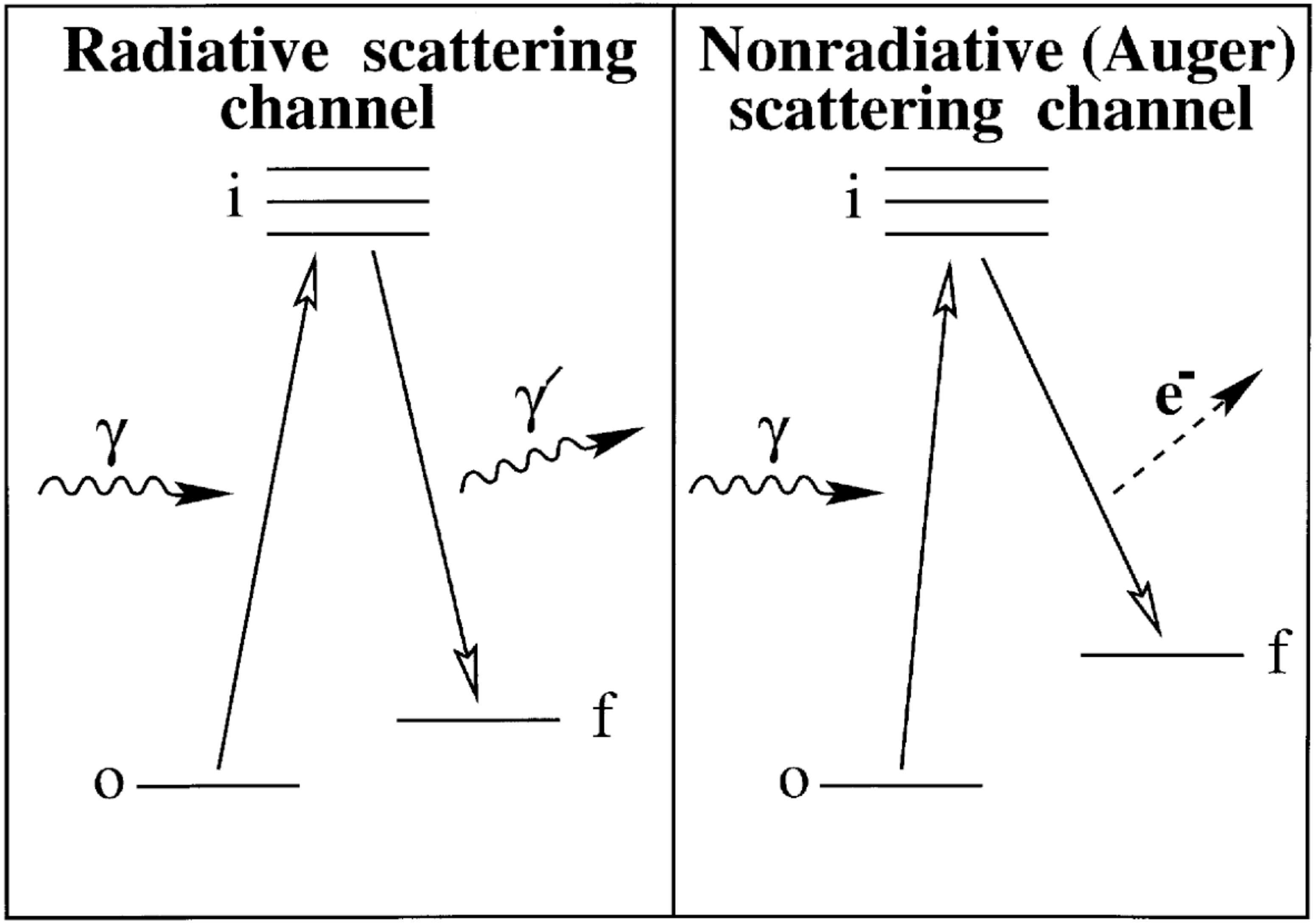

Fig. 1. Radiative (a) and non-radiative (b) X-ray Raman scattering.

Resonant Auger relaxation after inner shell resonant excitation.

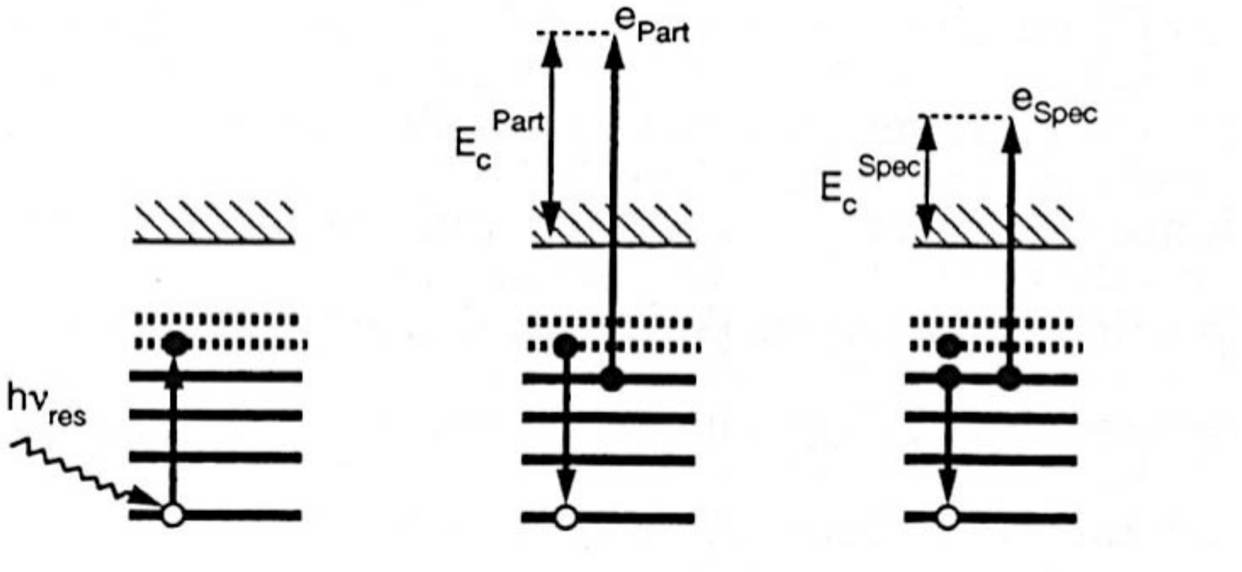

(1) (2) (3)

(1) : Inner shell resonant excitation. (2) Participator resonant Auger. (3) Spectator resonant Auger.

With moderate resolution, the resonant Auger lines are broadened by the corehole lifetime broadenings.

With the development of Synchrotron Radiation facilities (2^{nd} and 3rd) generation, the SR brilliance became very high.

Parallely, electron analysers and x-ray emission spectrometers became performant

→ High resolution spectra became measurable

Surprises arrived…

Resonant Raman Scattering: the width become less broad.

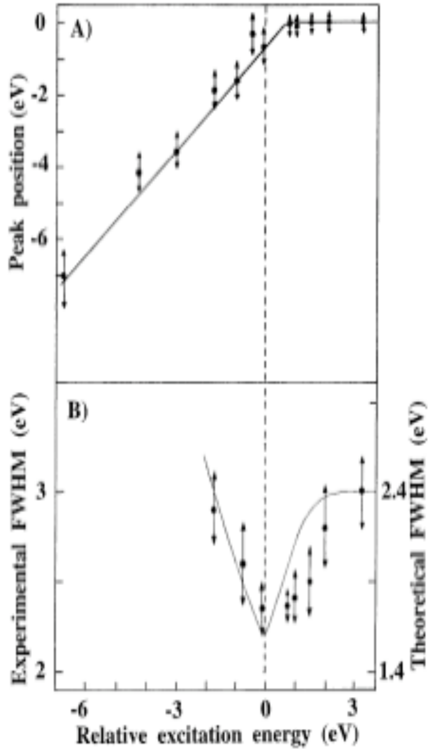

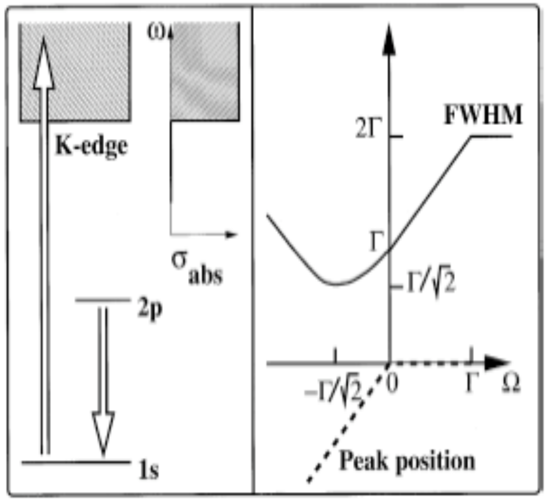

Comparison experiment/theory $K_{\alpha 2}$ of coper.

Eisenberger et al., Phys. Rev. Lett 36 (1976) 623

Auger Raman resonant

Photoelectrons

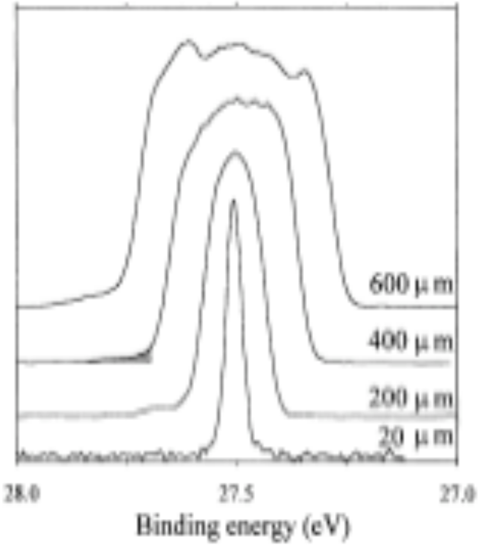

Kr 4s photoelectron spectra, recorded using different monochromator exit slit corresponding to different photon bandwidth.

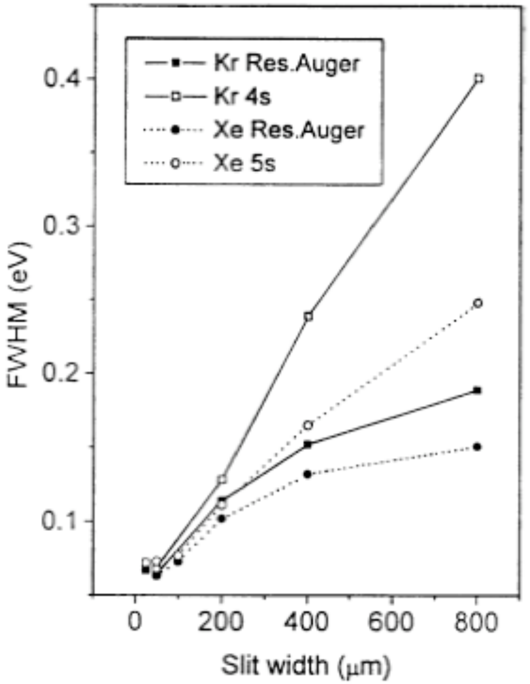

The width of the Kr and Xe resonant Auger lines, Kr 4s and Xe 5s photolines as a function of slit size

A. Kivimaki et al., Phys. Rev. Lett. 71 (1993) 4307

Kramers-Heisenberg formula : $\sigma(\omega,\omega_1) \propto \sum_k \left| \frac{\langle f|D'|k\rangle\langle k|D|i\rangle}{\omega_1 - \omega_{kf} - i\Gamma_k} \right|^2$

i: initial state

k : intermediate state

f : final state

Γ_k : lifetime broadening of the intermediate state

Excitation and relaxation cannot be considered as a two step mechanism.

The excitation and the relaxation occur simultaneously.

PHYSICS REPORTS

Physics Reports 312 (1999) 87–330

Resonant X-ray Raman scattering

Faris Gel'mukhanov, Hans Ågren

Out of several possible acronyms we prefer to use RXS – resonant X-ray scattering or resonant X-ray Raman scattering, and so radiative and non-radiative RXS. RIXS and REXS define inelastic and elastic (radiative) RXS, respectively. For the special case of non-radiative RXS with spectator decay we have occasionally also used RPE – resonant photoemission.

The primary requirement to conduct an RXS experiment is to have a narrowband source of tunable X-ray radiation available, to have tunable monochromators and an equipment for measuring RXS cross sections for different scattering angles and for different polarization (or spin) of incident X-ray photons and final particles. It is necessary that the light source has high intensity, and that the spectrometers are equipped for high resolution.

Resonant X-ray scattering (RXS) occurs due to an interaction of X-ray photons with a target consisting of atoms, molecules or a solid – for convenience we refer here to the target as a "molecule". The molecule is excited from the ground state $|o\rangle$ to a core excited state $|i\rangle$ by absorption of the incoming X-ray photon (γ) with frequency ω, wave vector $\boldsymbol{p}$ and polarization vector $\boldsymbol{e}$. The core excited state is metastable due to vacuum zero vibrations or interelectron Coulomb interaction and can therefore decay to final states $|f\rangle$ in two different ways. In the first type of decay channel a final X-ray photon (γ') with frequency ω', wave vector $\boldsymbol{p}'$ and a polarization vector $\boldsymbol{e}'$ is emitted

$$M + \gamma \rightarrow M_i \rightarrow M_f + \gamma' \ . \tag{2}$$

The energy of the core excited state can also be released by ionization of one of the electrons e^- of the molecule:

$$M + \gamma \rightarrow M_i \rightarrow M_f + e^- \ . \tag{3}$$

These two decay channels constitute the radiative and the non-radiative X-ray scattering processes, respectively. When the frequency of the incident X-ray photons is tuned below or closely above the core ionization threshold resonant, core excitation takes place. It is natural to refer to this case as to resonant X-ray scattering (RXS) or X-ray Raman scattering.

The RXS process thus consists of two steps. In the first step the molecule absorbs an X-ray photon and in the second step it emits a final particle, an X-ray photon or an Auger electron. The processes and the energy relations are sketched in Fig. 1 and described in detail in this review.

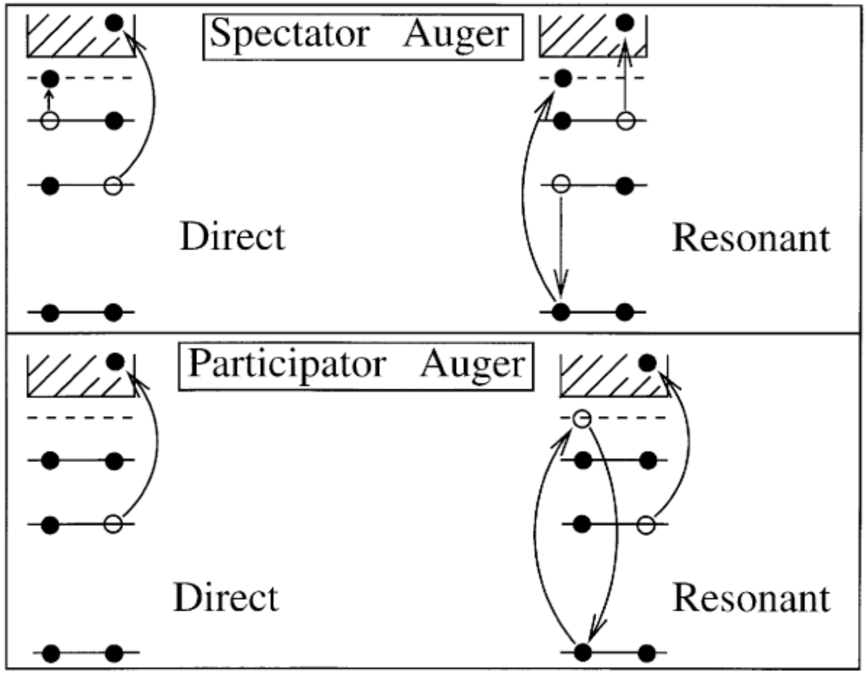

Fig. 8. Non-resonant and resonant contributions to non-radiative RXS (resonant photoemission or resonant Auger effect).

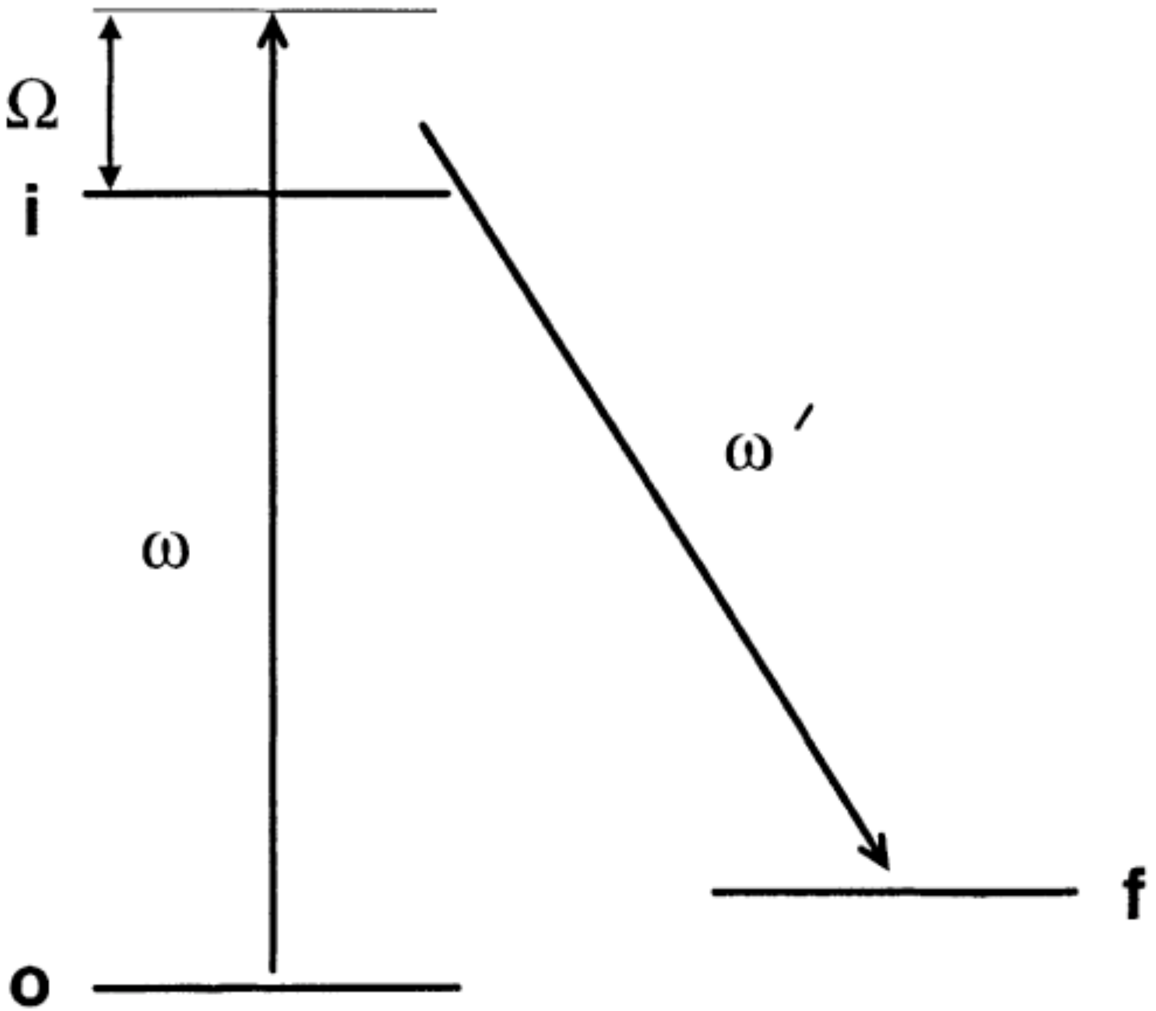

Fig. 14. A 3-level model for RXS.

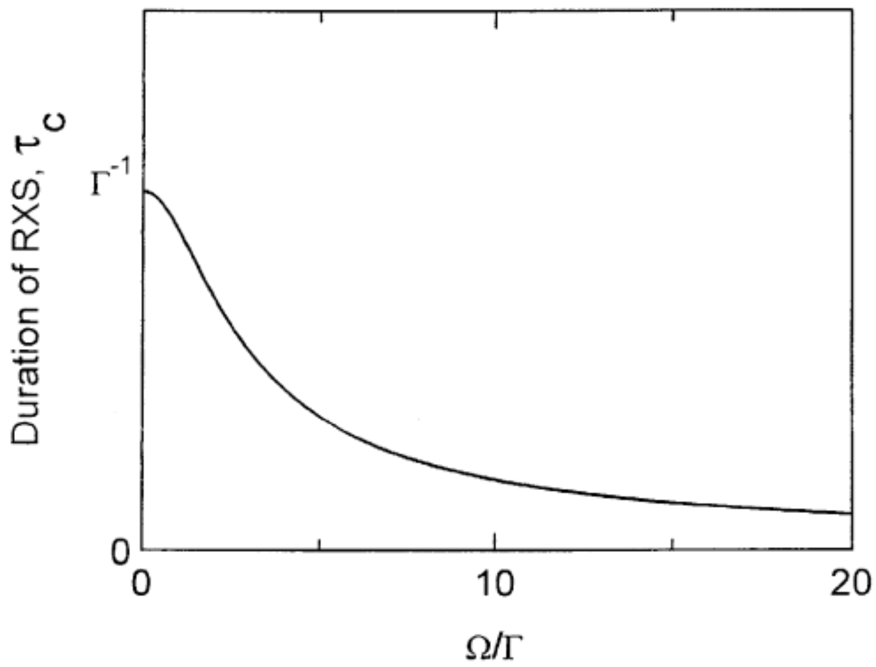

Fig. 21. Dependence of the RXS duration τ_c on the excitation energy (40).

Core hole clock spectroscopy

Using the core hole lifetime to measure a fast process (nuclear motion, fragmentation, Charge Transfer…)

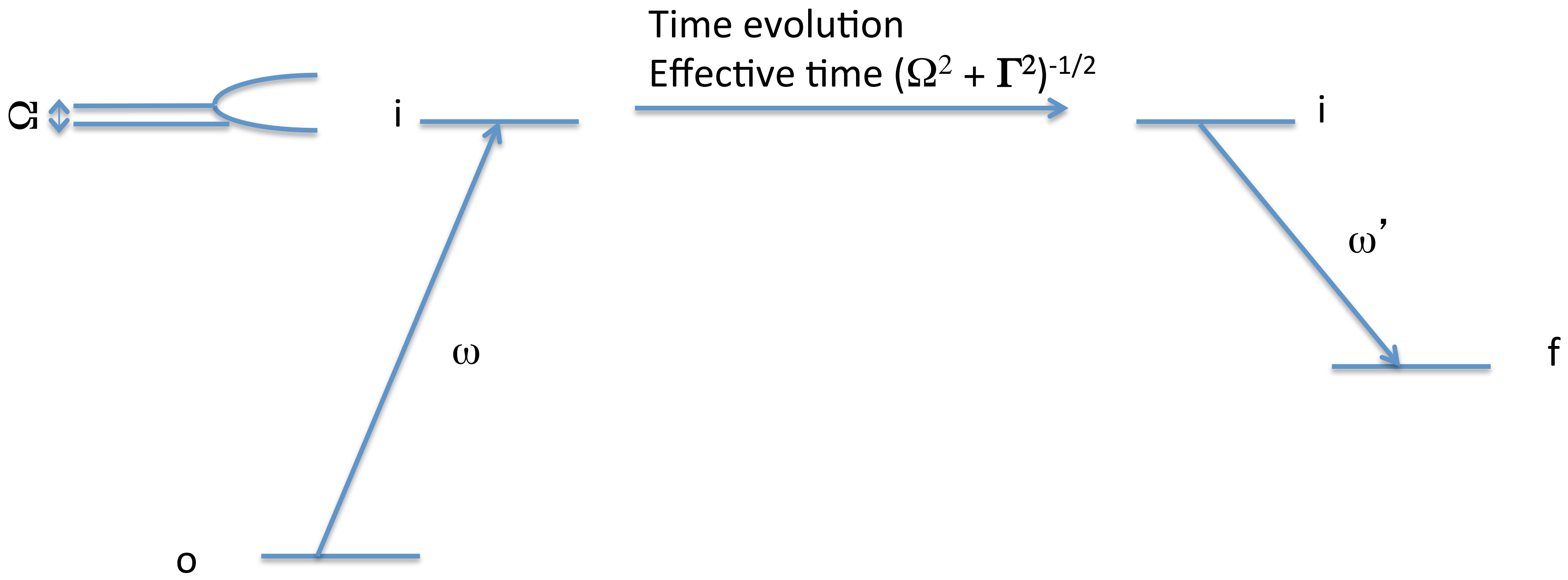

Time evolution

Effective time $(\Omega^2 + \Gamma^2)^{-1/2}$

In the soft x-ray domain, lifetime are in the order of a few femtoseconds
In the hard x-ray domain, lifetime are equal or lower than one femtosecond

Actual State of the art Instrumentation

The best synchrotron beamlines can now reach a resolving power between 10000 and 100000. Typically 1meV at 100 eV.

High Resolution Electron analysers are commercially available (resolution better than 10 meV).

Intense competition in development of x-ray emission spectrometers. The best spectrometer has a resolving power of 10000.
(50 meV at 500 eV).

Ultrafast fragmentation observed in the soft X-rays

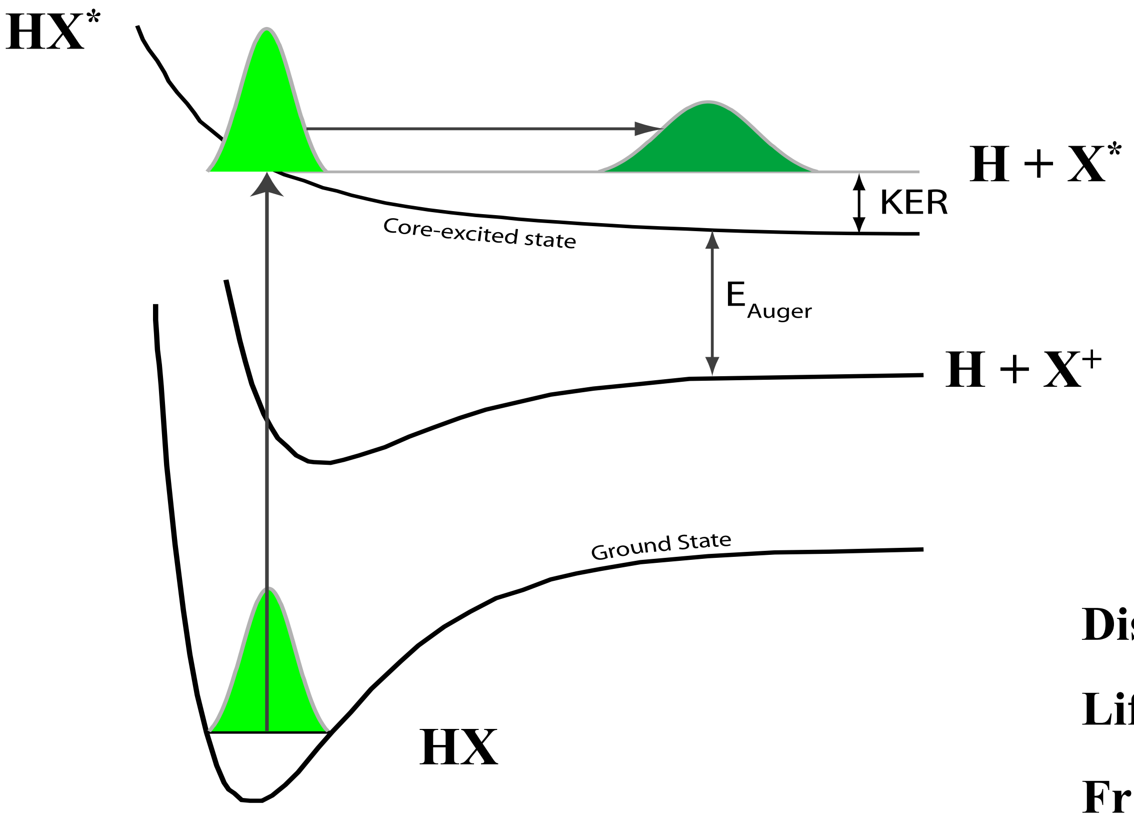

Dissociative core excited state

Lifetime of several femtoseconds

Fragment emission

X= Br, Cl, I, F, NH_2, OH, HS, CH_2Cl, SiH_3, CH_2F...

O_2 , SF_6

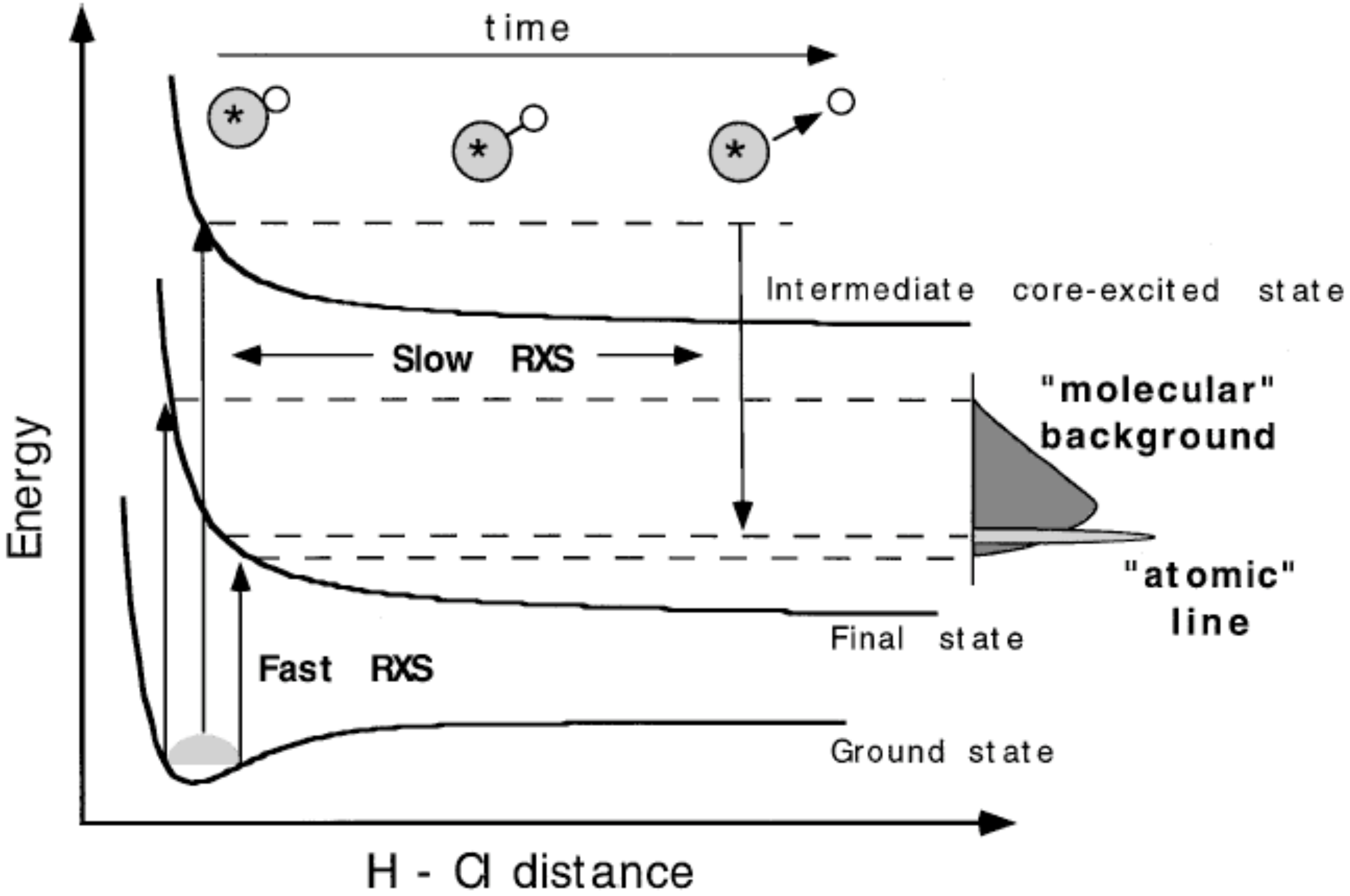

FIG. 1. A simple picture of the formation of the atomic and molecular line profiles in resonant x-ray scattering spectra involving a dissociative core-excited state.

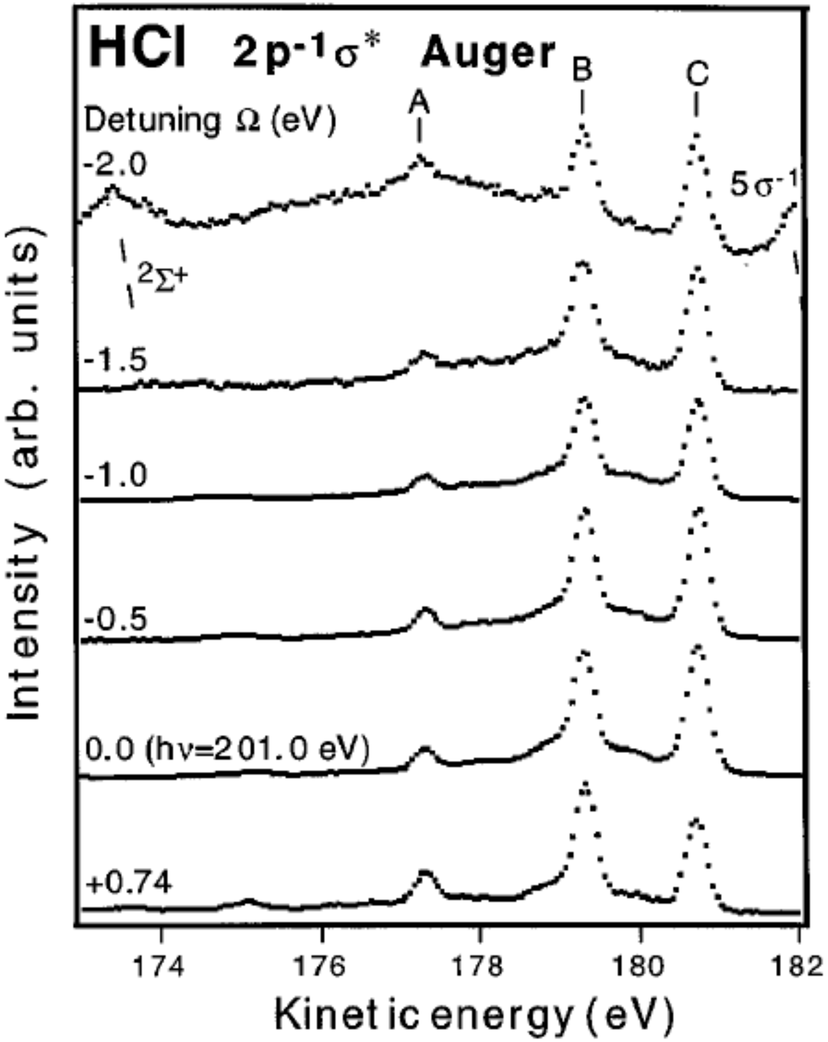

FIG. 2. Experimental resonant Auger spectra, showing the $2p_{3/2}^{3}3p^{6} \rightarrow 3p^{4}, 2p_{1/2}^{1}3p^{6} \rightarrow 3p^{4}$ region of the atomic Auger decay transitions in HCl as function of detuning.

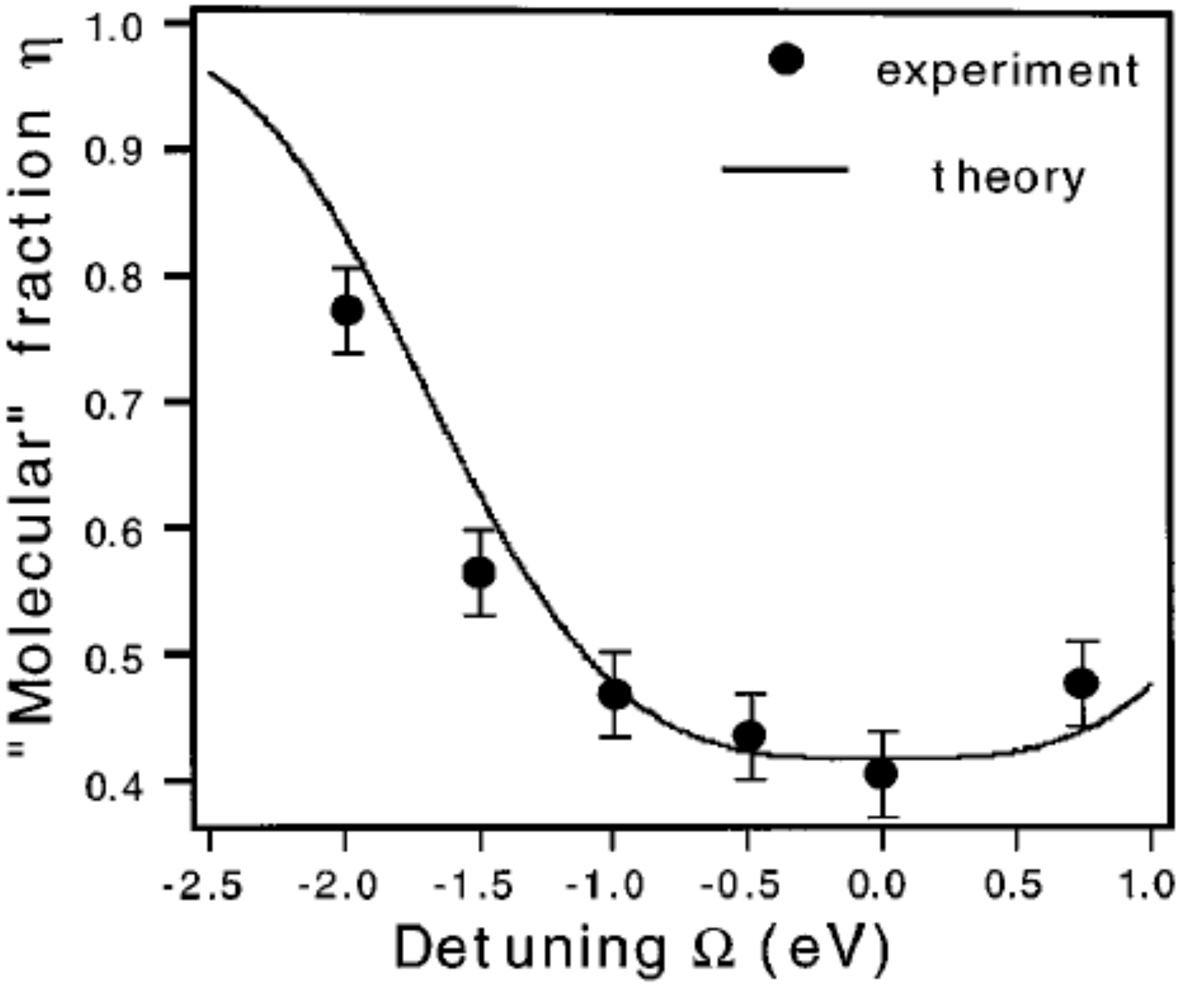

FIG. 3. Comparison of the experimental and theoretical fraction η of the molecular background to the total Auger intensity.

Doppler Splitting of In-Flight Auger Decay of Ultrafast Dissociating Oxygen Molecules

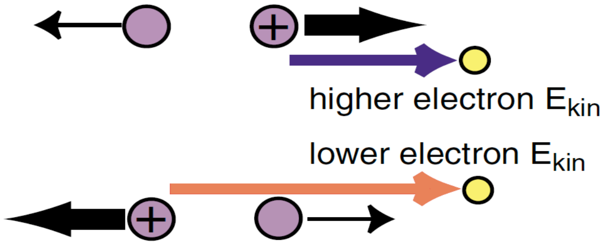

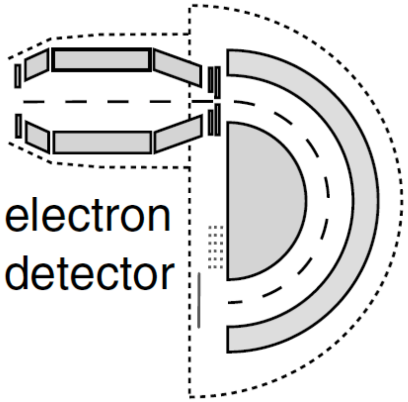

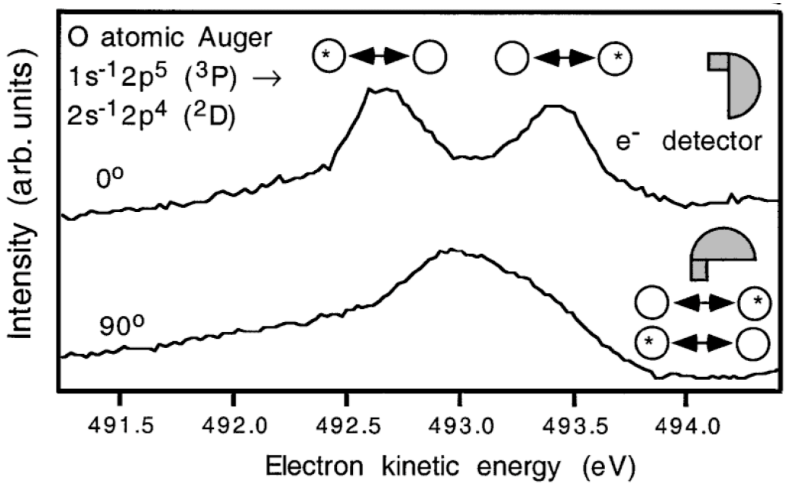

General effect predicted by F. Gel'mukhanov et al., Phys. Rev. A (1998) and first observed on O_2 by O. Bjorneholm et al., Phys. Rev. Lett. (2000)

Observed on O_2, O_3, CF_4, CH_3F, SF_6, doubly excited CO…

Intermolecular electron scattering and electron transfer after primary emission.

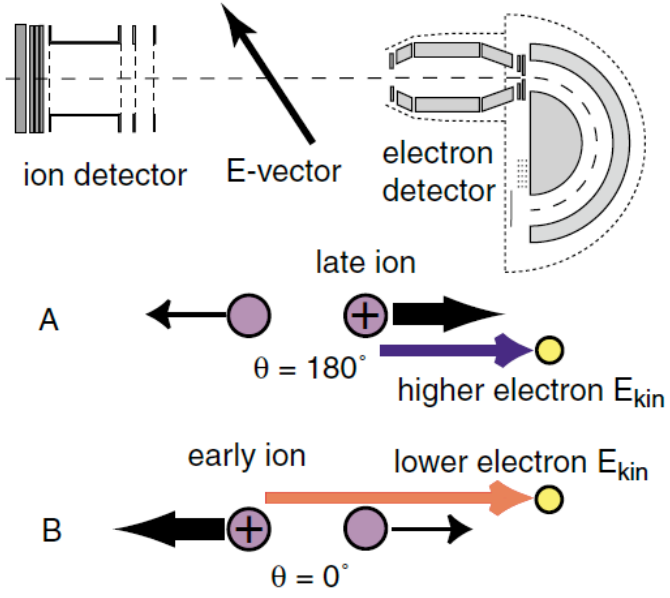

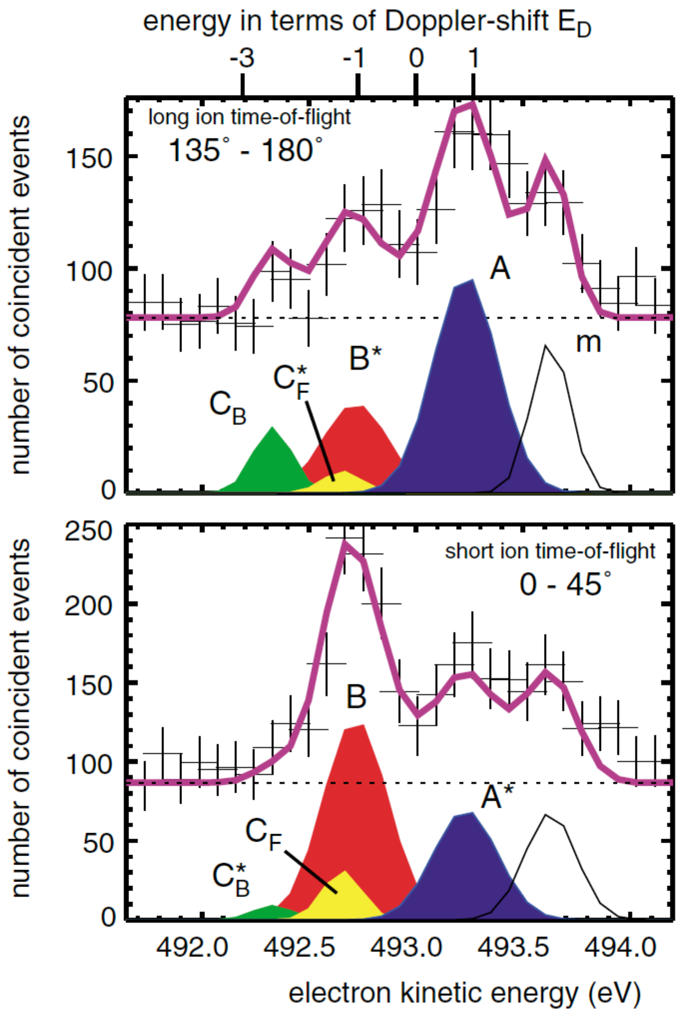

O. Kugeler, G. Prümper, R. Hentges, J. Viefhaus, D. Rolles, U. Becker, S. Marburger and U. Hergenhahn
Phys. Rev. Lett. 93 033002 (2004)

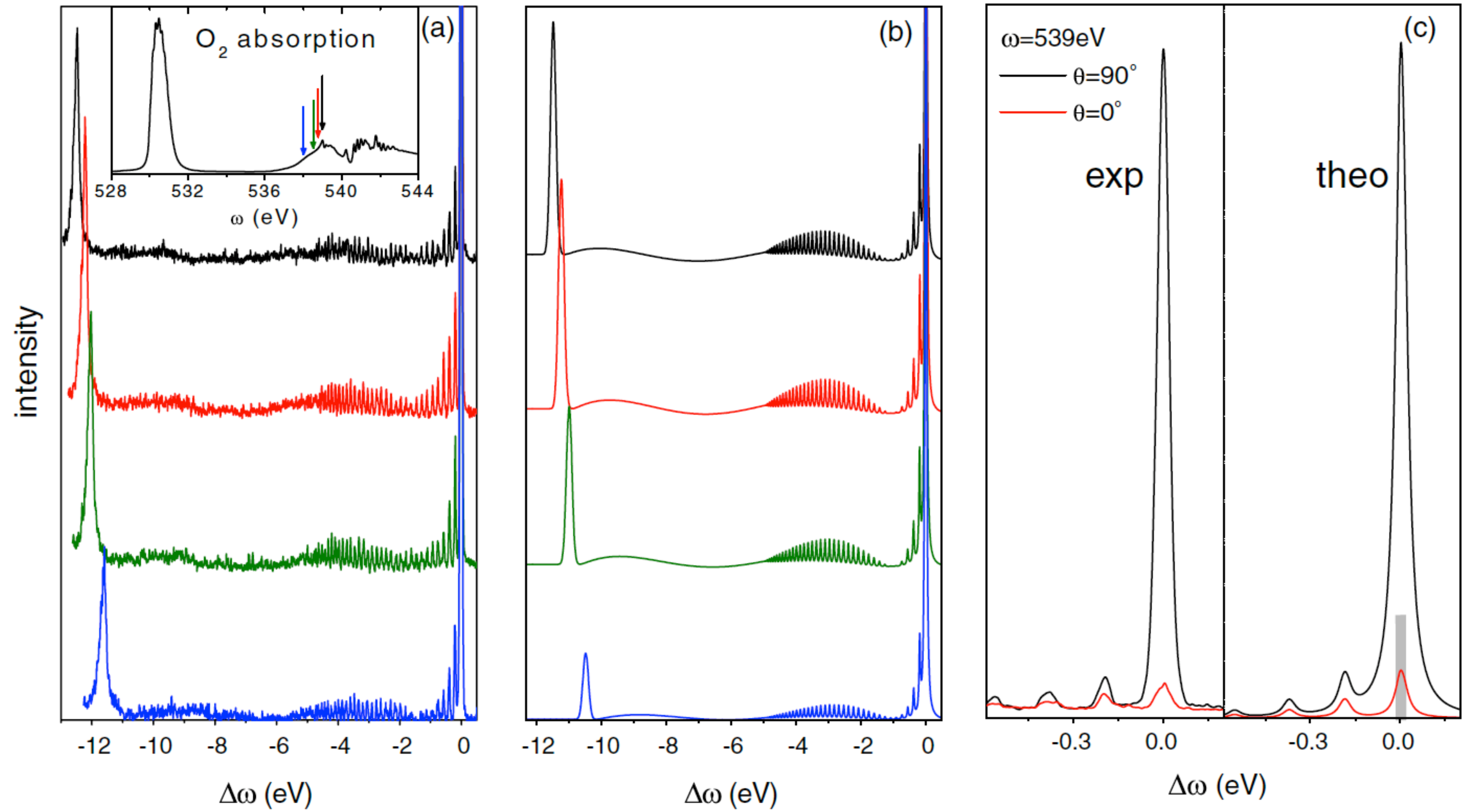

FIG. 1 (color online). Experimental (a) and theoretical (b) RIXS spectra for $\theta = 90^\circ$; $\omega = 539, 538.75, 538.5, 538$ eV (from top to bottom) as indicated in the absorption spectrum in the top panel. The theoretical "atomic" peak includes also contribution from the dissociative $1^3\Pi_g$ final state which converges to the same dissociative limit as the ground state. The polarization dependence of the RIXS spectrum shown in panel (c) demonstrates that scattering to $\nu = 0$ has a different dependence on the angle $\theta = \angle(\mathbf{e}, \mathbf{n}_1)$ (here $\theta = 0^\circ$ and 90°), than scattering to $\nu > 0$. The gray bar shows the intensity of the elastic peak intensity for $\theta = 90^\circ$ without Thomson scattering.

A. Pietzsch et al., Phys. Rev. Lett. 106, 153004 (2011)

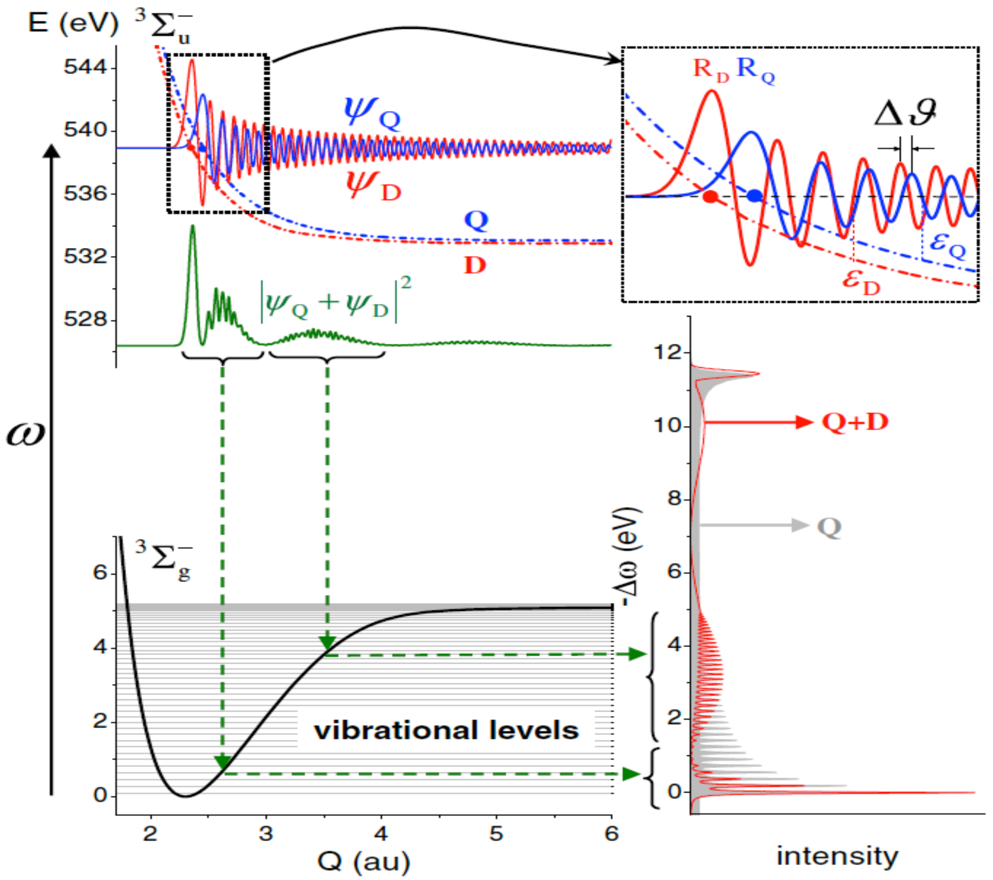

FIG. 2 (color online). Physical picture of the modulations in the vibrational RIXS spectrum. The calculated RIXS spectrum (gray profile in the right panel) with one intermediate state does not display any envelope oscillations and differs qualitatively from the experimental spectrum. The interference between the Q and D scattering channels results in a spatial modulation of the total wave packet $\Psi_Q + \Psi_D$ which leads to the beat structure in the RIXS spectrum ("$Q + D$" spectrum in the right panel). The reflection principle explains qualitatively how the spatial modulation of $|\Psi_Q + \Psi_D|^2$ gives the intensity modulation in the RIXS spectrum.

A. Pietzsch et al., Phys. Rev. Lett. 106, 153004 (2011)

Ultrafast nuclear motion of core excited molecules

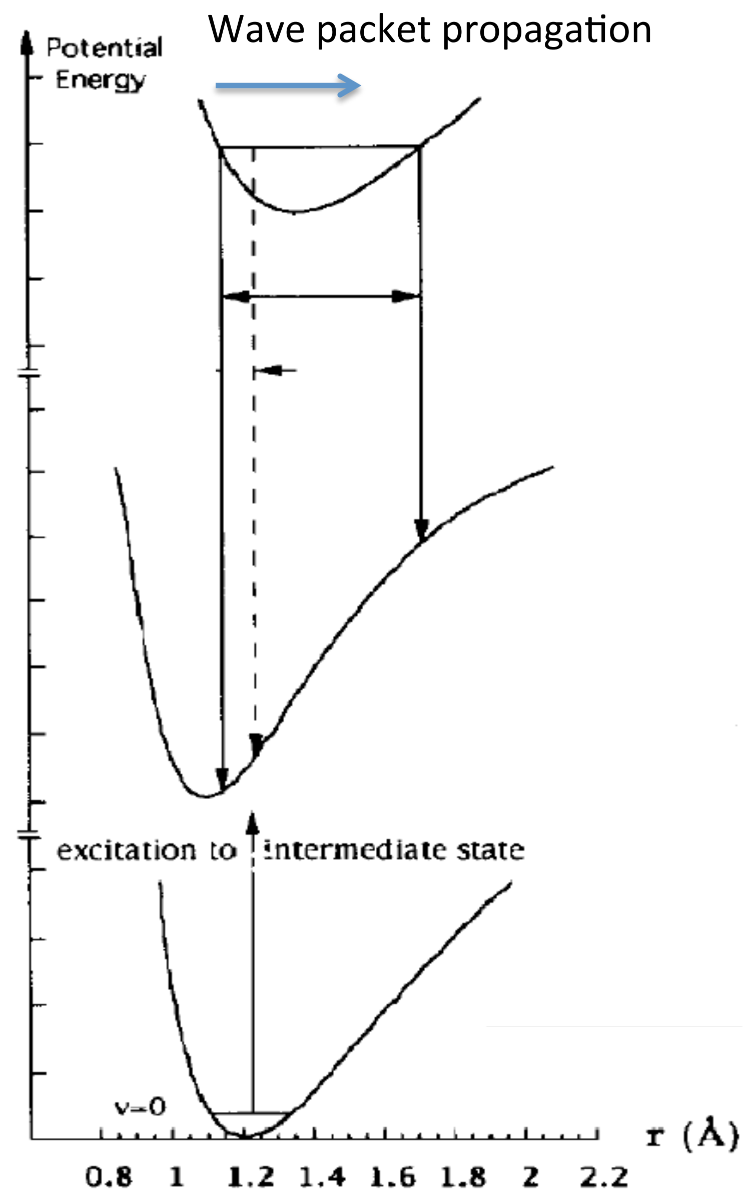

Resonant excitation of the BF_3 molecule around the boron K edge: PEPIPICO measurements

Fragmentation of doubly charged ions

B1s -> $2a_2''$

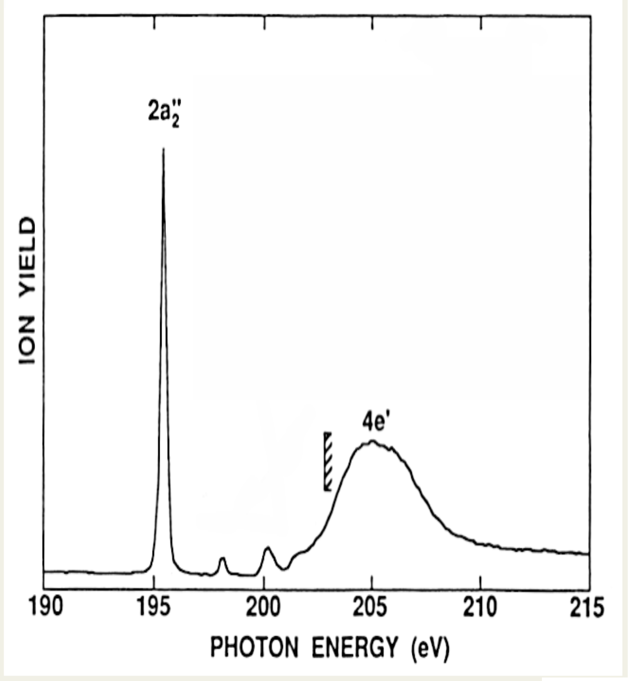

B1s -> $2a_2''$

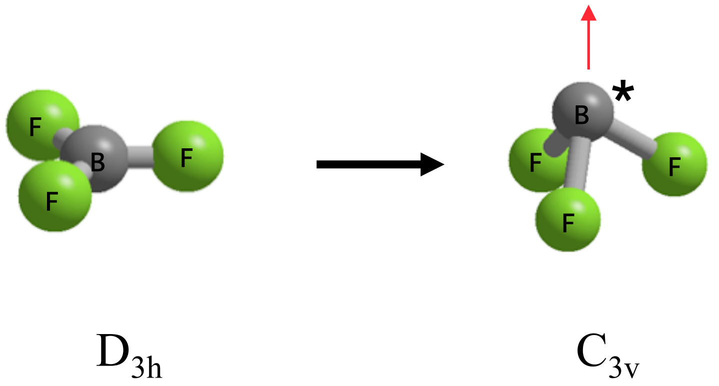

B1s -> $2a_2''$

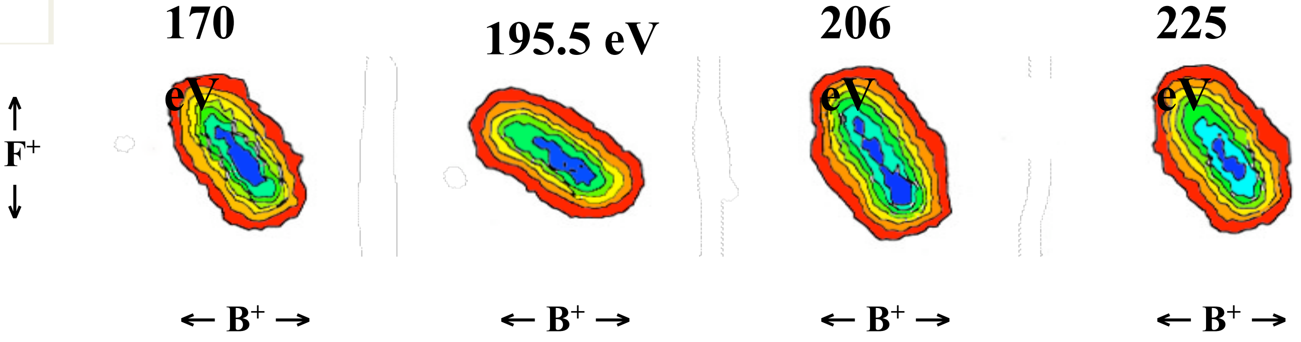

M. Simon et al., Chemical Physics Letters 238, 42 (1995)

Dynamical Auger process observed on the BF_3 molecule excited around the Boron 1s edge

Lifetime : several femtoseconds

Geometry change within the intermediate state

Dynamical Auger emission

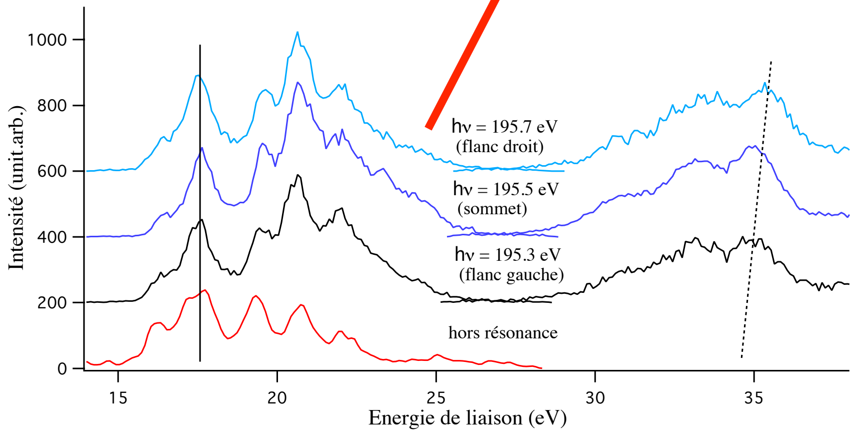

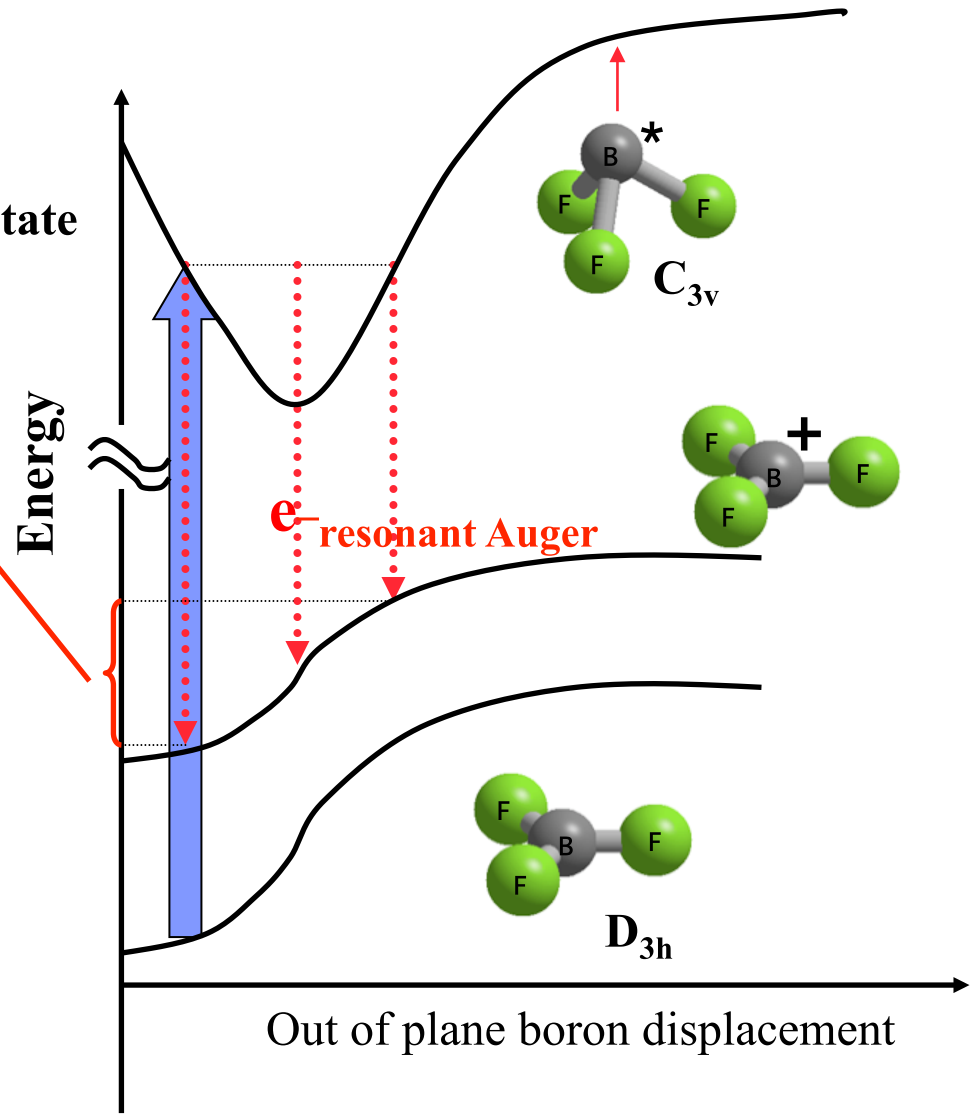

M. Simon et al., Phys. Rev. Lett. (1997)

Imaging Potential Energy Surfraces. The N_2 case.

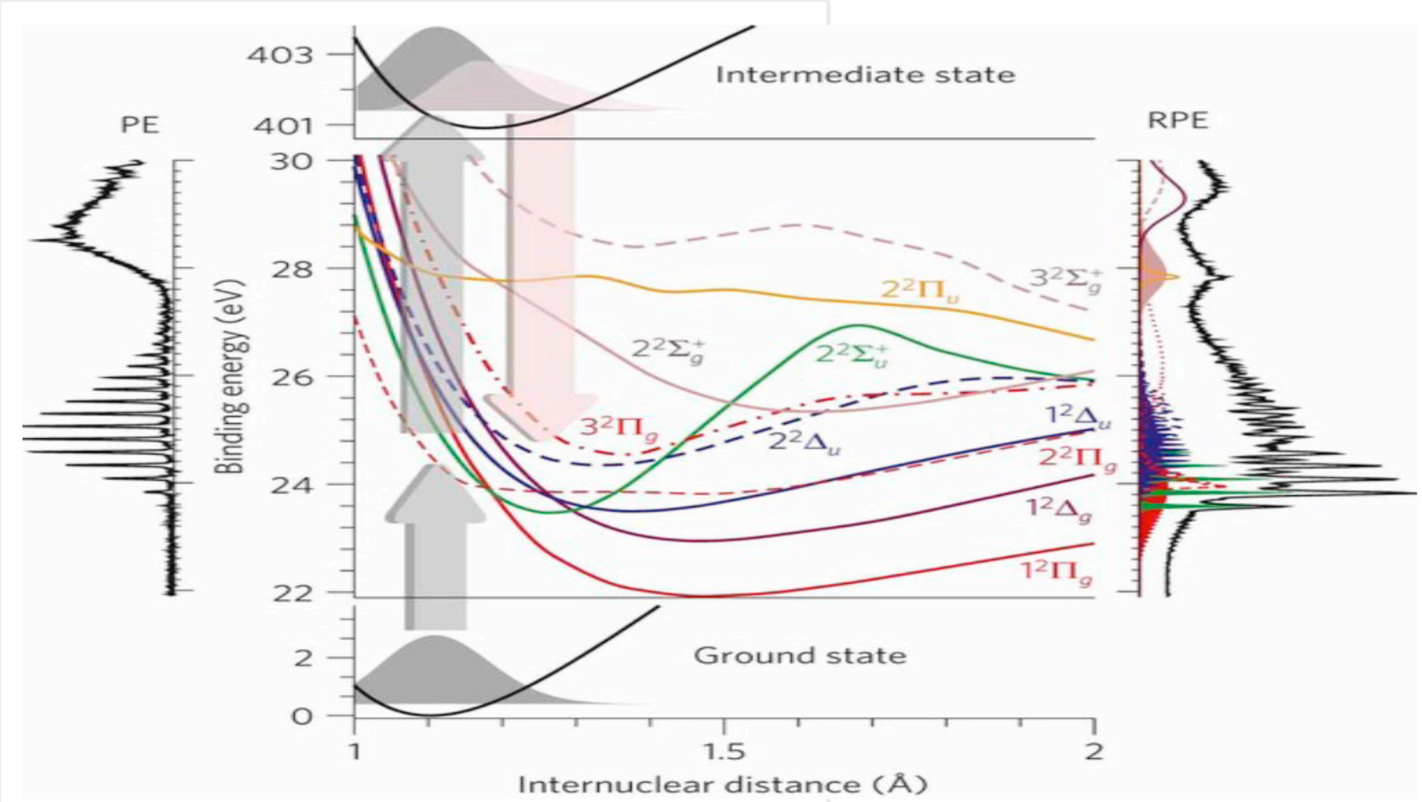

Ab initio calculated potential-energy curves of the ground, intermediate (core-excited) and final ionic (N_2^+) states are shown in the central panel. A strong congestion of states can be observed around the vertical transition from the zero-point vibrational level of the ground electronic state shown by the ascending grey arrow. In addition to the resulting spectral band overlap, some states are 'dark' in the photoemission spectrum recorded at 100 eV photon energy (left-hand panel). The ground-state nuclear wave packet excited to the intermediate-state potential (grey) continuously undergoes Auger decay (pink) to final ionic states, as indicated by the descending pink arrow. Owing to the nuclear dynamics in the core-excited state, the decay takes place at larger internuclear distances, providing the opportunity to visualize the potentials in a region free of any overlap. Experimental and calculated partial

C. Miron et al. Nature Physics **8**, 135–138 (2012)

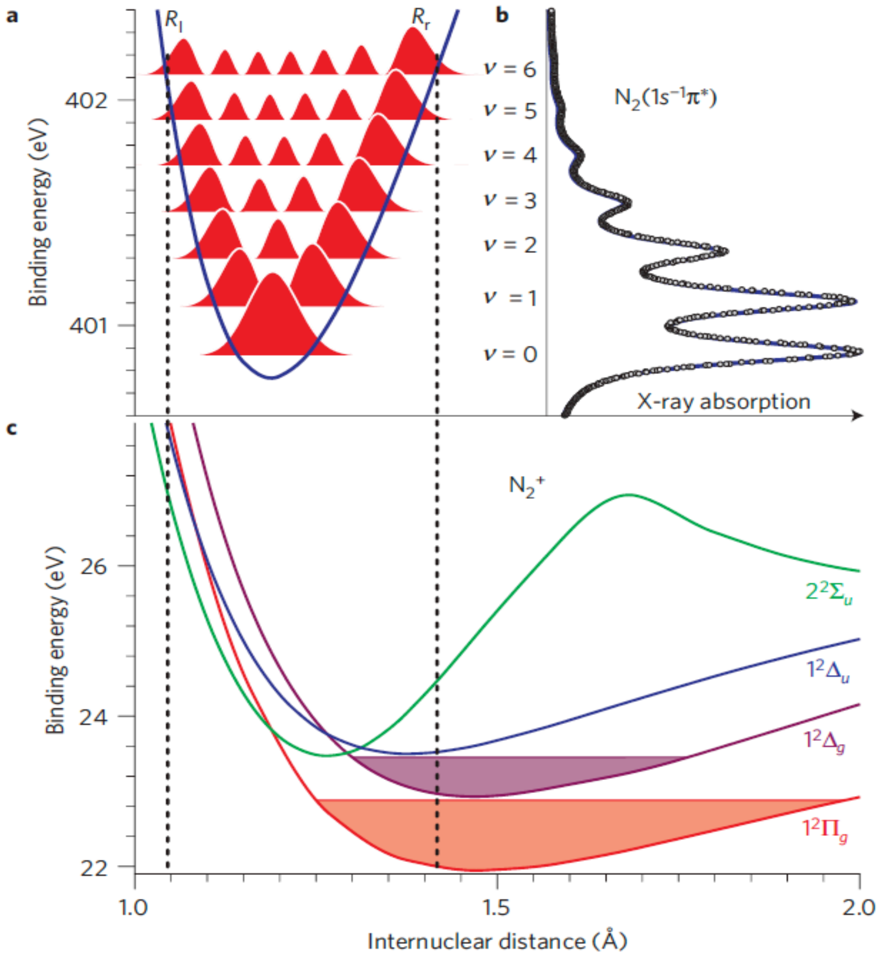

Figure 3 | Controlling the extension of the vibrational wavefunctions in the intermediate core-excited state through the X-ray photon energy. **a**, Calculated potential of the $1s^{-1}\pi^*$ core-excited state and the squares of the vibrational wavefunctions of the first vibrational substates. Left (R_l) and right (R_r) classical turning points are shown for $\nu = 6$. **b**, Experimental (circles) and theoretical (solid line) N $1s \to \pi^*$ X-ray photoabsorption spectra of nitrogen molecule. **c**, Selected final ionic-state potentials that can be explored in the region free of mutual overlap are shown by the shaded areas.

C. Miron et al. Nature Physics **8**, 135–138 (2012)

State of the art : RIXS with Vibrational Resolution

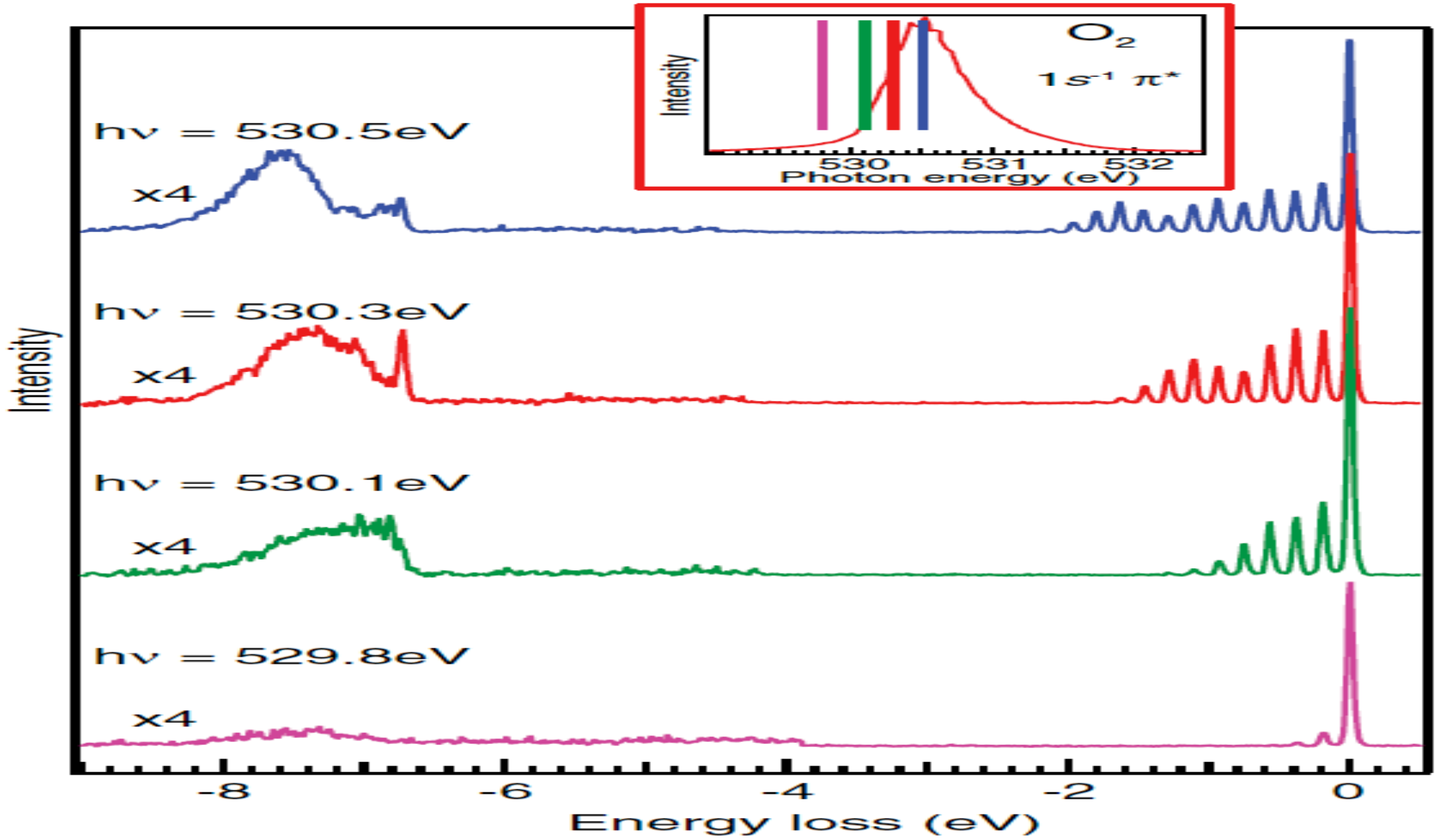

F. Hennies, A. Pietzsch, M. Berglund, A. Föhlisch, T. Schmitt, V. Strocov, H. Karlsson, J. Andersson, and J.-E. Rubensson, *Phys. Rev. Lett. 104, 193002 (2010)*

Bent cristal spectrometer developped for a bright source

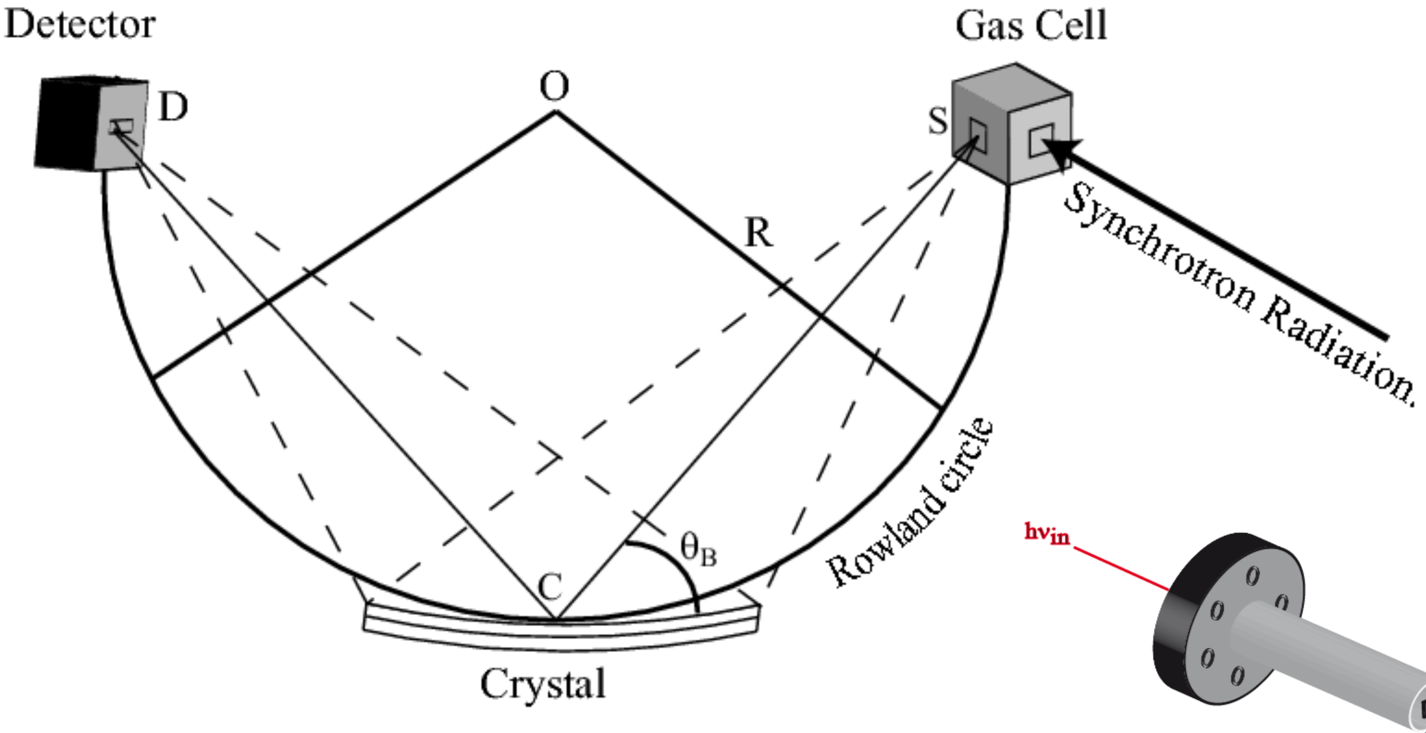

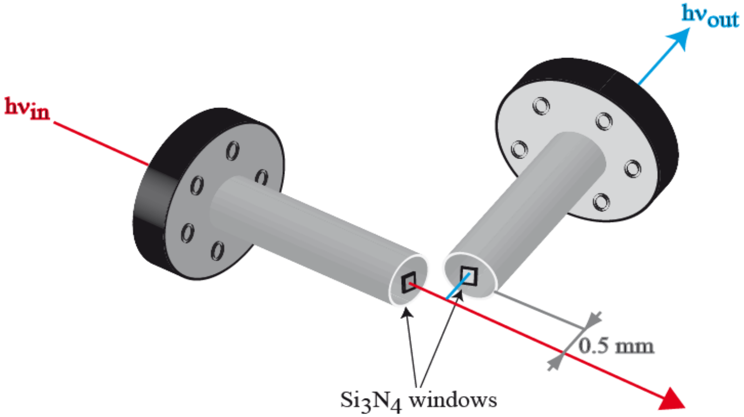

Polarization measurements
Reabsorption limited
Angular distribution
Resolution : 500 meV at 3 keV

L. Journel et al., Rev. Sci. Instrum. 80, 093105 (2009)

Elastic peak broadened by nuclear motion

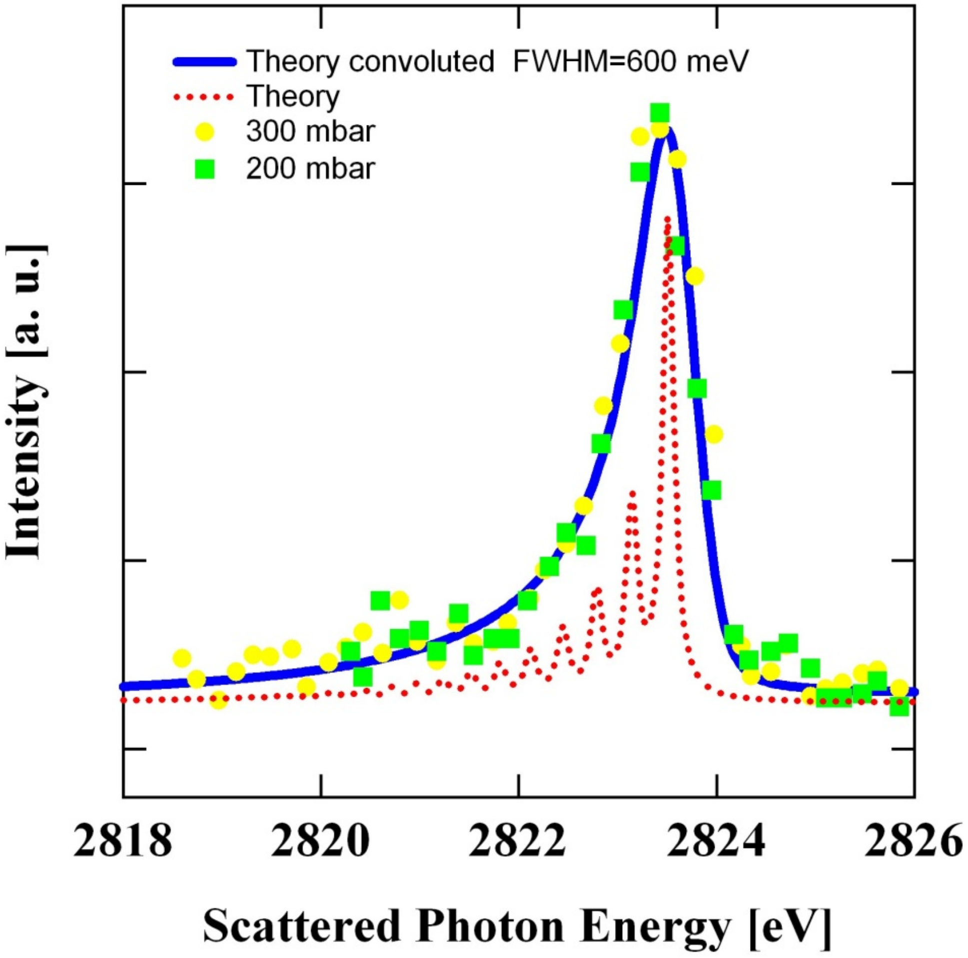

Core hole lifetime : 1.05 fs

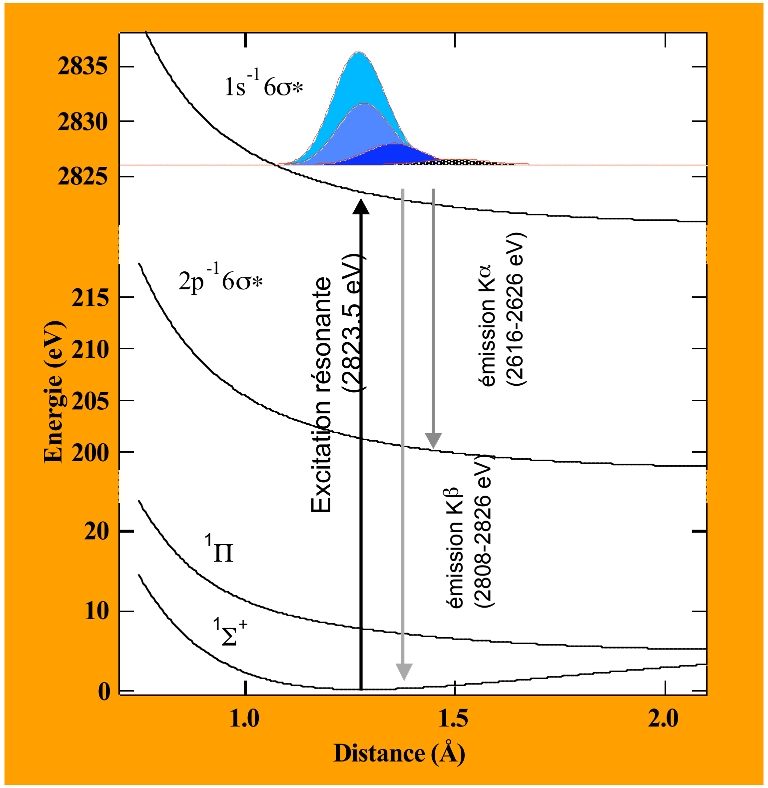

Chemical bond elongation: 10 picometers within 1 femtosecond

M. Simon et al., Phys. Rev. A 73 (2006) 020706

Resonant Inelastic X-ray Scattering

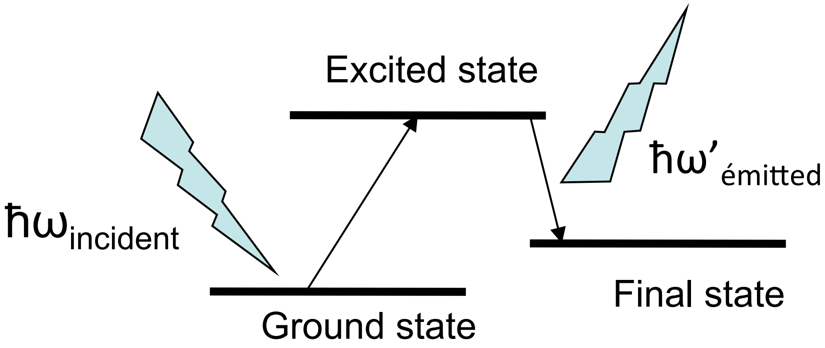

Kramers-Heisenberg

$$\sigma(\omega,\omega') \propto \sum_c \left| \frac{\langle f|\vec{\varepsilon}'.\widehat{D}|c\rangle\langle c|\vec{\varepsilon}.\widehat{D}|i\rangle}{\omega'-\omega_{cf}+i\Gamma_c} \right|^2$$

Excitation and relaxation within one step

- Two photons spectroscopy
- Chemical selectivity
- Strict selection rules
- Neutral final state

Resolution for excitation (0.4 eV)

Résolution for analysis (0.3 eV)

$$\left.\begin{matrix} \\ \\ \end{matrix}\right\} < \Gamma_c = 0{,}64\ \text{eV}$$

Raman Resonant

Regime

ω' : emitted energy

ω_{cf} : energy of the radiative transition

Γ_c = natural width of the intermediate state

Absorption spectrum of the HCl molecule around the K edge

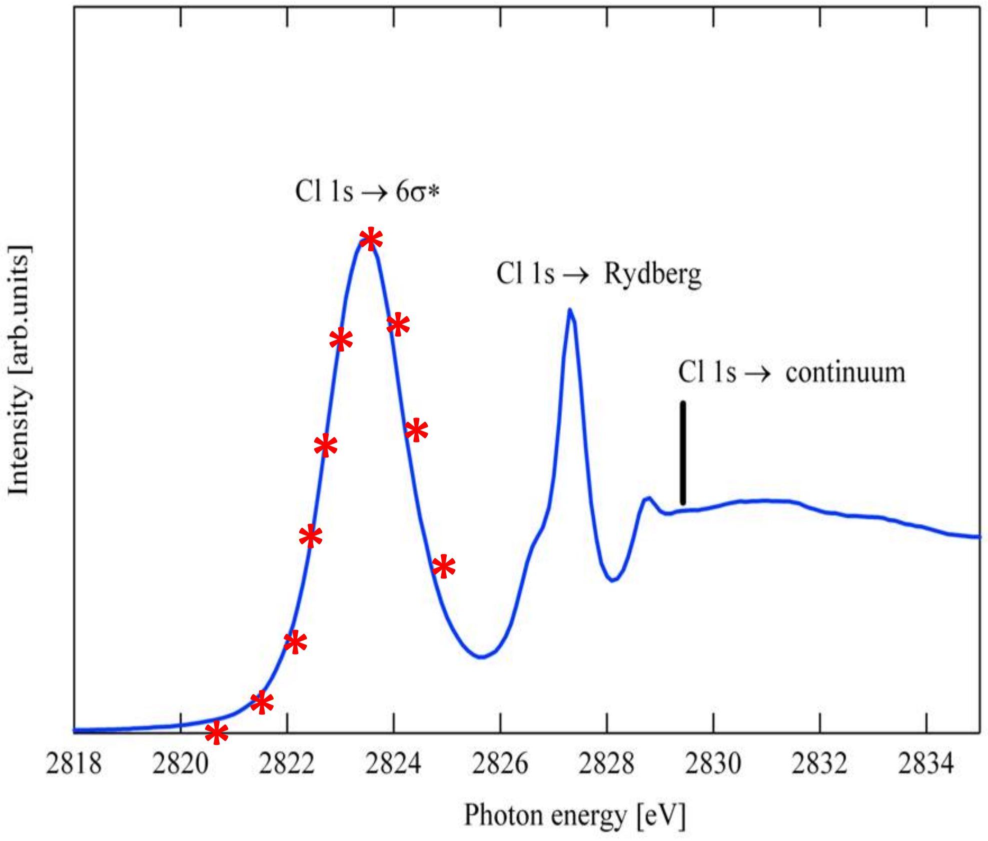

Absorption spectrum of gas-phase HCl around the Cl 1sthreshold.

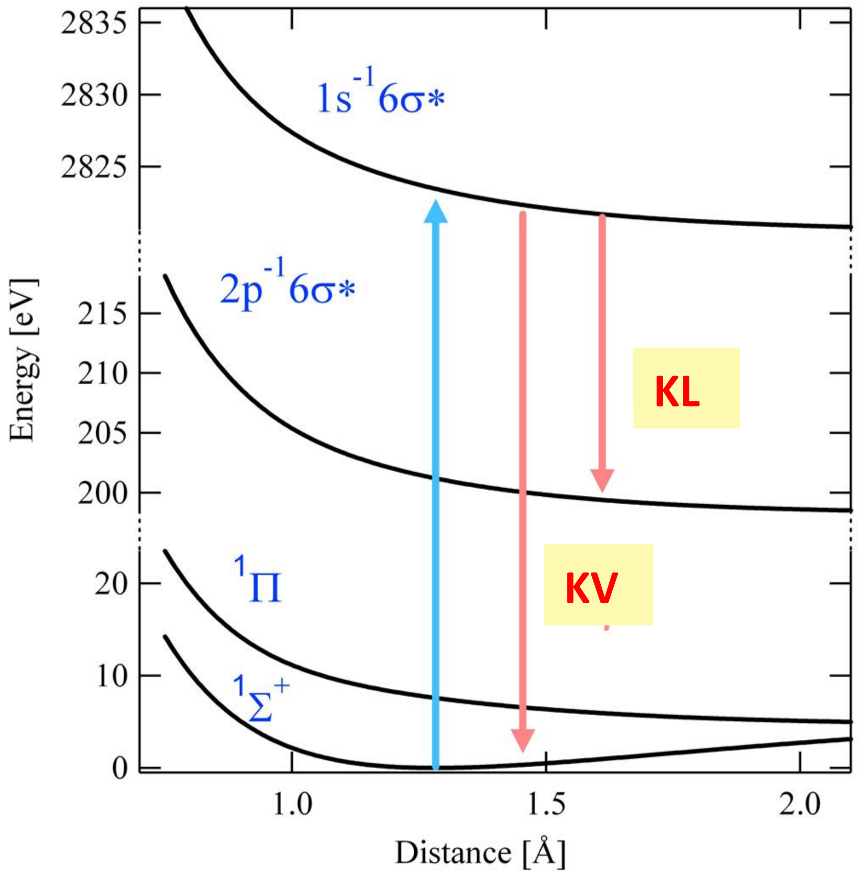

Potential Energy Curves DFT

Resonant Kα emission of the HCl molecule

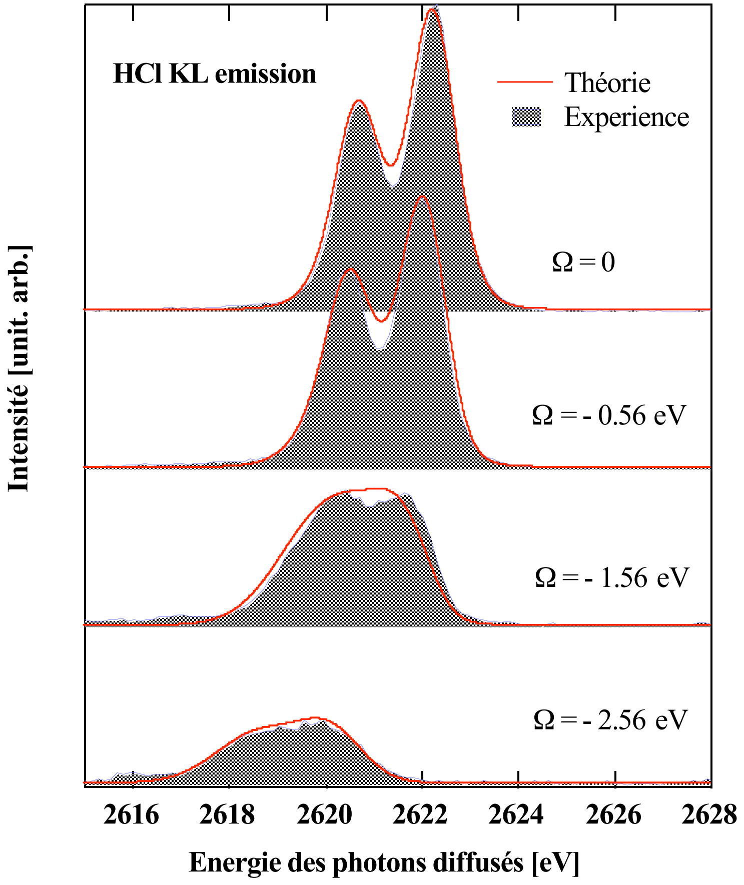

2 spin-orbit component:
$2p_{3/2}$ and $2p_{1/2}$

Width and dispersion depend

on the energy detuning ω.

Parallelism of $1s^{-1}\sigma^*$ and $2p^{-1}\sigma^*$ P.E.S.

$$\sigma(\omega,\omega_1) \propto \frac{\exp(-[(\omega_1-\omega)/\Delta]^2 \ln 2)}{\omega_1^{\,2} + \Gamma^2/4}$$

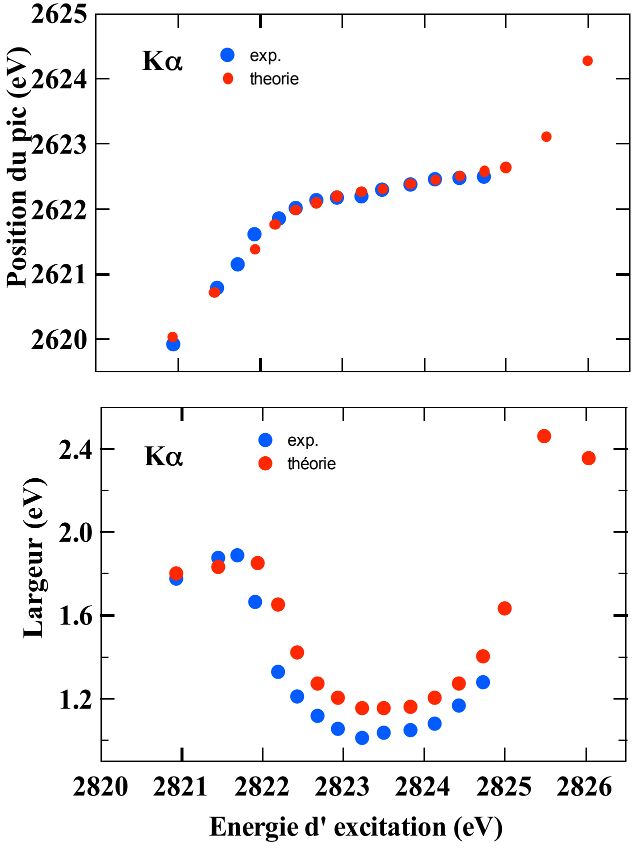

M. Simon et al., Phys. Rev. A 73, 020706 (2006)

General features for molecules in RIXS

Comparison with atomic RIXS

In CF_3Cl, $(1s^{-1})$ and $(2p^{-1})$ have parallel PES.

General conclusion: RIXS in molecules driven by the topology of PES of the initial, intermediate, and final states.

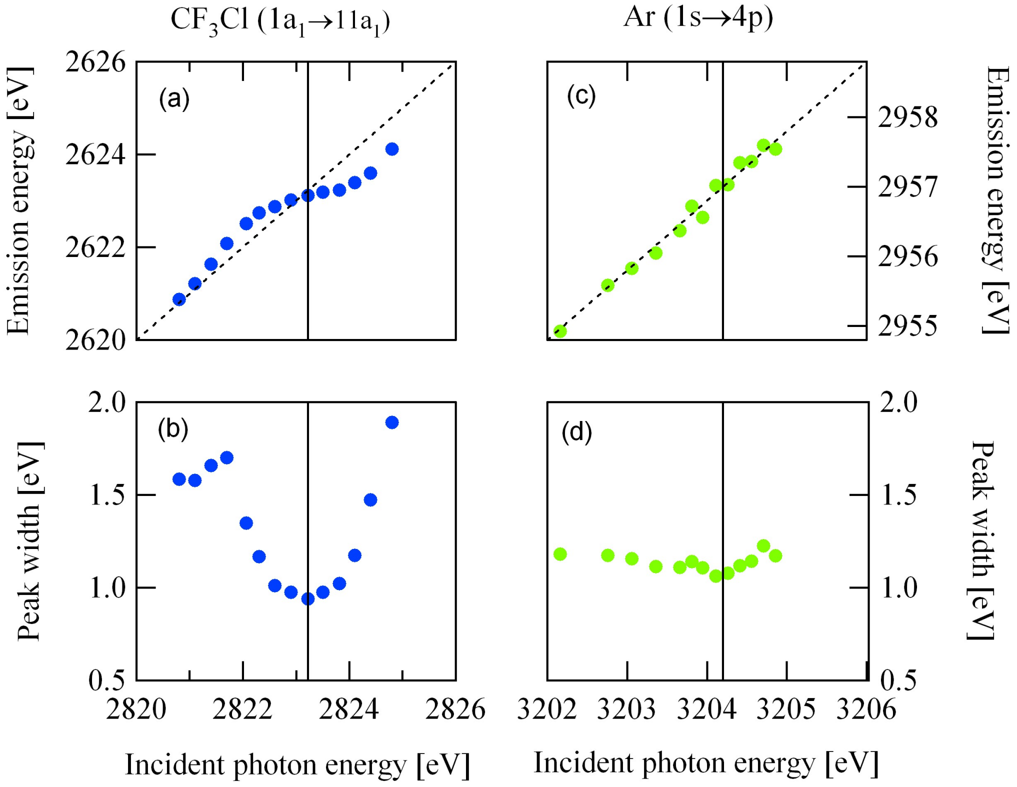

Excitation-emission interferences in resonant x-ray emission after K-shell excitation in HCl

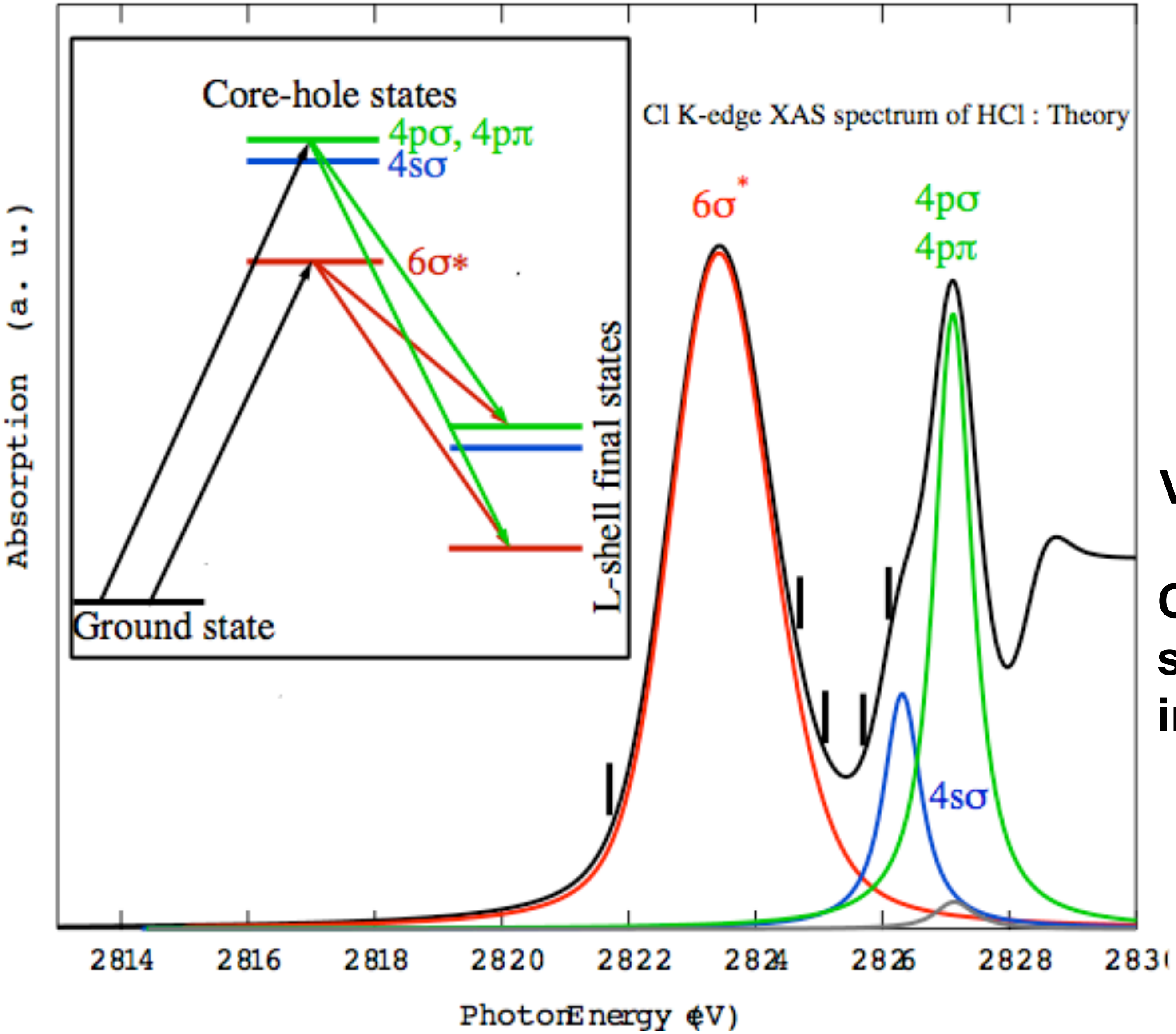

Very short lifetime : 1 fs

Coherent excitation of several electronic intermediate states

Excitation-emission interferences in resonant x-ray emission after K-shell excitation in HCl

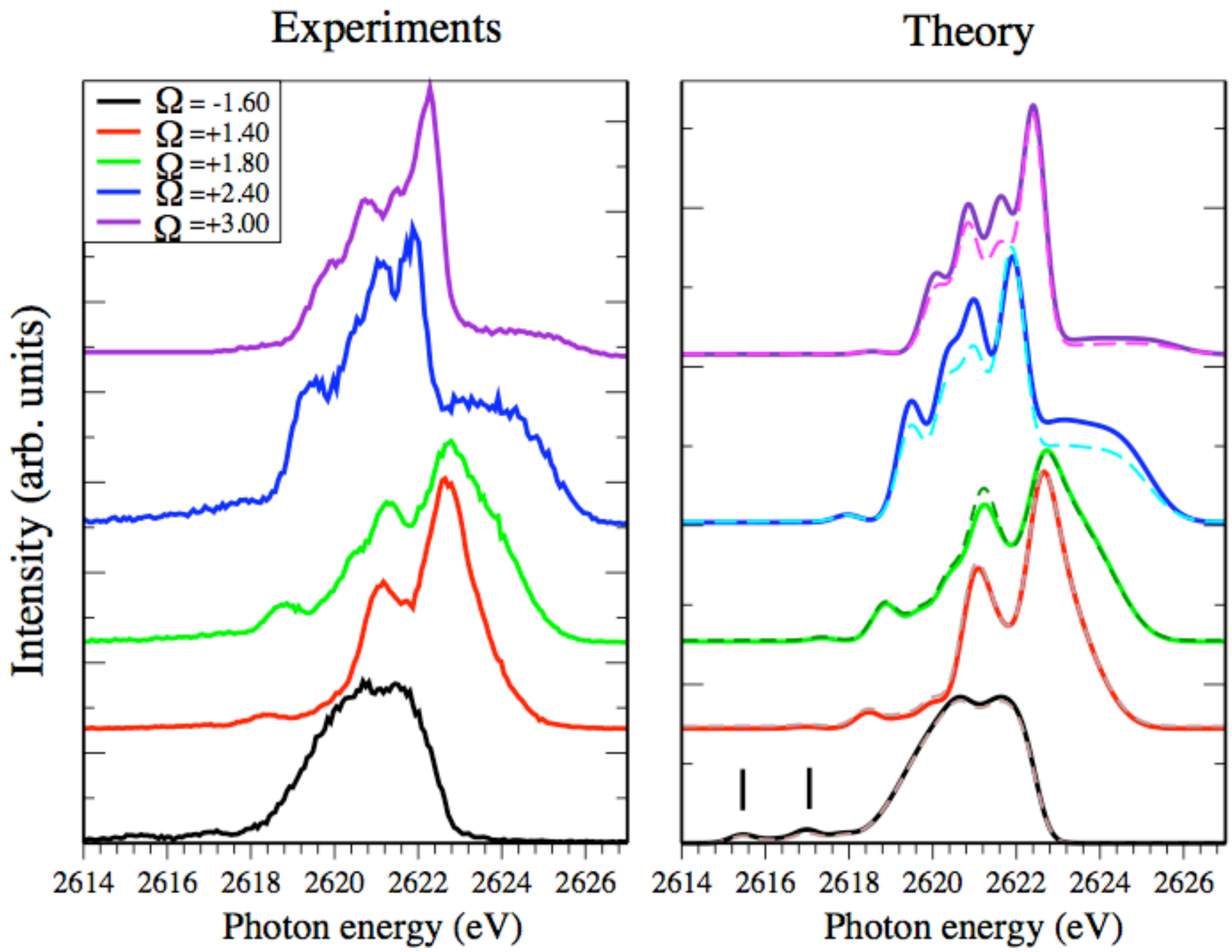

—— with interferences

------ without interferences

M. Kavcic et al., Phys. Rev. Letters (2010)

Ultrafast Charge Transfer

Sulfur Atoms chemisorbed on Ruthenium

S_{2s} core hole lifetime : 500 attoseconds

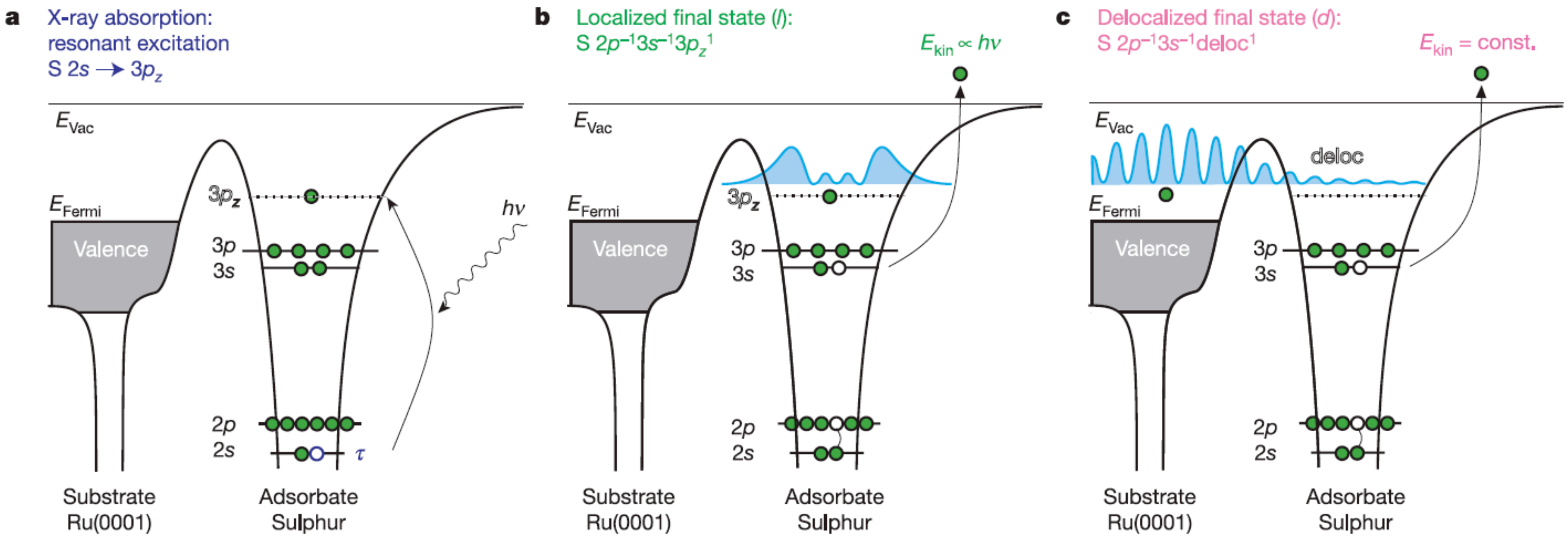

Figure 1 | Core-hole clock spectroscopy—schematic overview. a, Initially, a core electron is promoted by resonant excitation from the S 2*s* level into a bound resonance localized at an adsorbed sulphur atom ($S\,2s^{-1}3p_z^1$) on ruthenium c(4 × 2)S/Ru(0001) with a core-hole lifetime $\tau = 0.5$ fs. In the autoionization decay processes, Coster–Kronig decay of the S 2 *s* core hole takes place in the presence of this electron, the so-called 'spectator' electron, leading to two different final states. **b**, Localized final state $S\,2p^{-1}3s^{-1}3p_z^1$: state *l*. The initially excited electron is still localized at the sulphur atom. **c**, Delocalized final state $S\,2p^{-1}3s^{-1}\mathrm{deloc}^1$: state *d*. The initially excited electron has already left the localized resonance. E_{vac}, vacuum energy; E_{Fermi}, Fermi energy; E_{kin}, kinetic energy.

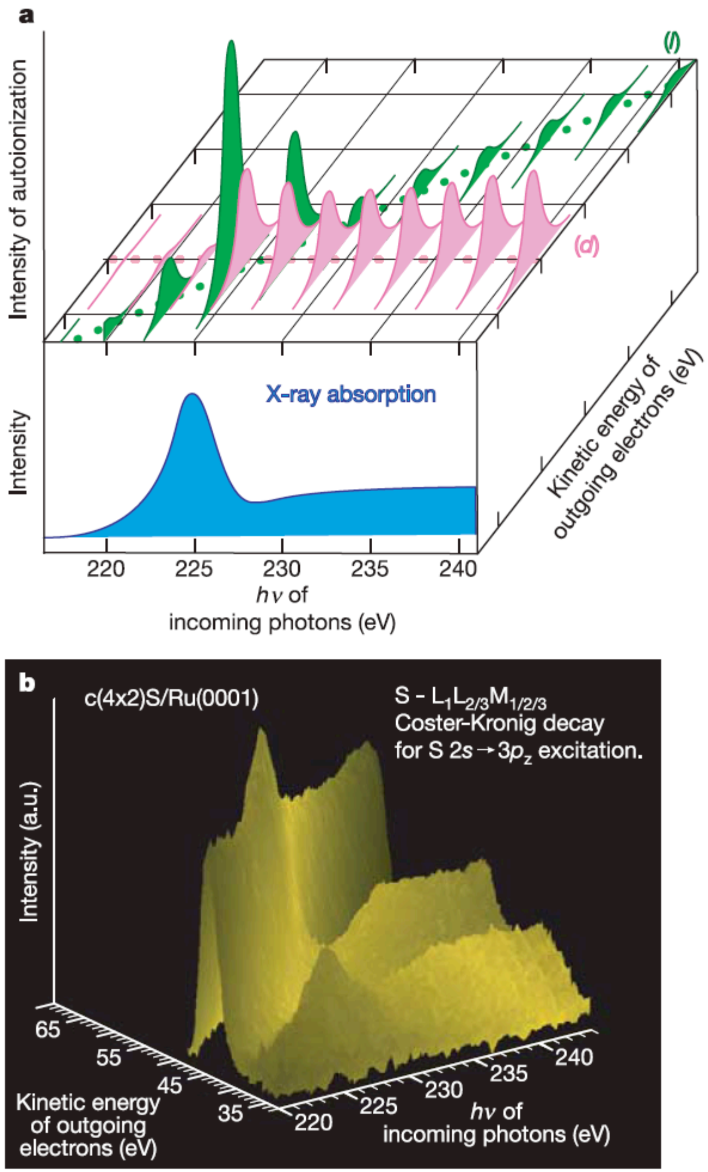

Figure 2 | Core-hole clock spectroscopy—the spectroscopic signatures. **a**, Diagram of the spectroscopic autoionization signatures leading to a localized final state (*l*) with linear dispersion and a delocalized final state (*d*) at constant kinetic energy, and their relation to resonant excitation by X-ray absorption. **b**, Experimental sulphur $L_1L_{2/3}M_{1/2/3}$ Coster–Kronig autoionization spectra of c(4 × 2)S/Ru(0001) as a function of incident photon energy.

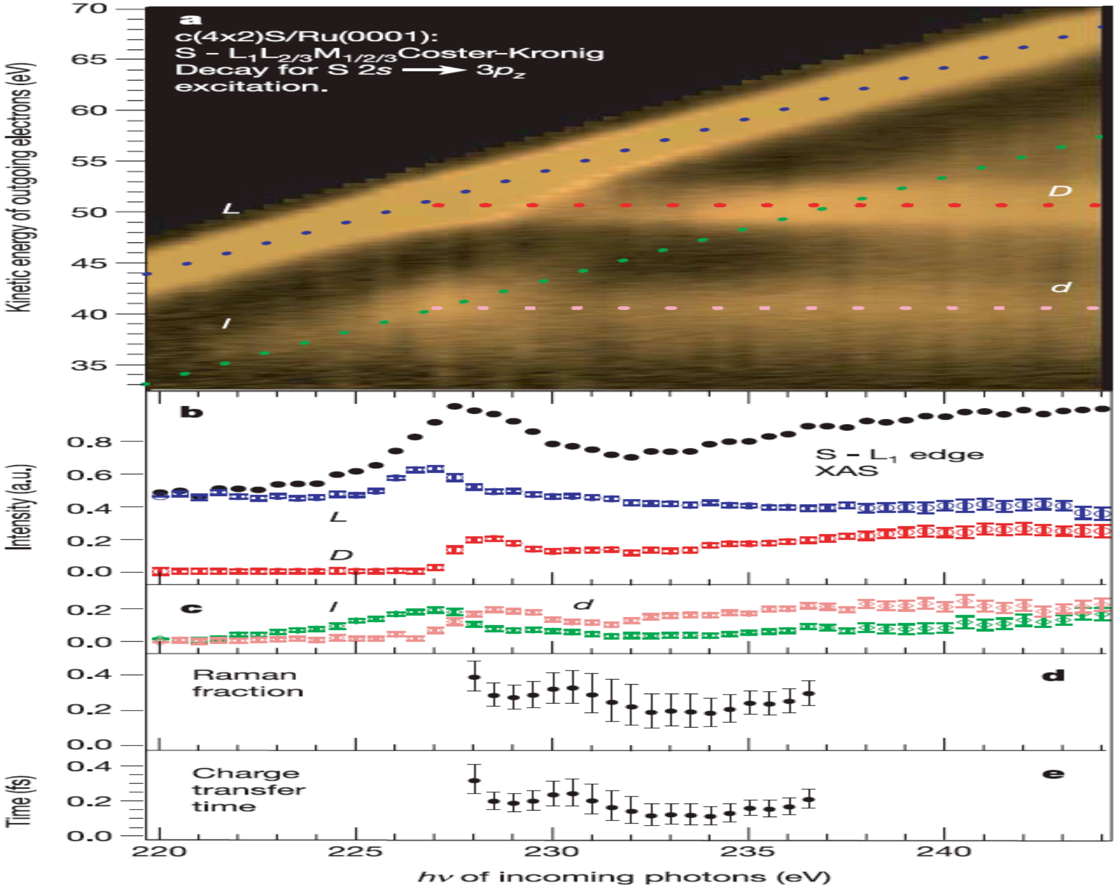

Figure 3 | Quantitative charge transfer analysis of sulphur $L_1L_{2/3}M_{1/2/3}$ Coster–Kronig autoionization spectra of c(4 × 2)S/Ru(0001) as a function of photon energy. **a**, Experimental intensities as a function of incoming photon energy and kinetic energy of the outgoing electrons. Lighter colours correspond to higher autoionization intensity. Shown are Raman channels with linear dispersion for localized final states L ($2p^{-1}3p^{-1}3p_z^1$) at 170.7 eV binding energy and l ($2p^{-1}3s^{-1}3p_z^1$) at 181.7 eV binding energy, and charge transfer channels with delocalized final states D ($2p^{-1}3p^{-1}\mathrm{deloc}^1$) at 50.8 eV kinetic energy and d ($2p^{-1}3s^{-1}\mathrm{deloc}^1$) at 40.6 eV kinetic energy. **b**, Sum of spectral intensities representing the S-L_1 edge X-ray absorption spectrum. Also shown are separate intensities of the spectral channels (L, D) from curve fitting with lorentzians of 3.3 eV FWHM. Error bars show the standard deviation of each fit. **c**, Separate intensities of the spectral channels (l, d) from curve fitting with lorentzians of 3.3 eV FWHM. Error bars show the standard deviation of each fit. **d**, Raman fraction $f = l/(l + d)$ as a function of photon energy. Error bars are derived from the standard deviation of the fits (see **c**). **e**, Charge transfer time obtained from the Raman fraction as $\tau_{CT} = \tau f/(1 - f)$ and the S 2s core-hole lifetime $\tau = 0.5$ fs. Error bars are derived from the standard deviation of the fits (see **c**).

A. Föhlisch et al. Nature **436**, 373 (2005)

Polarised RIXS: influence of Molecular Field

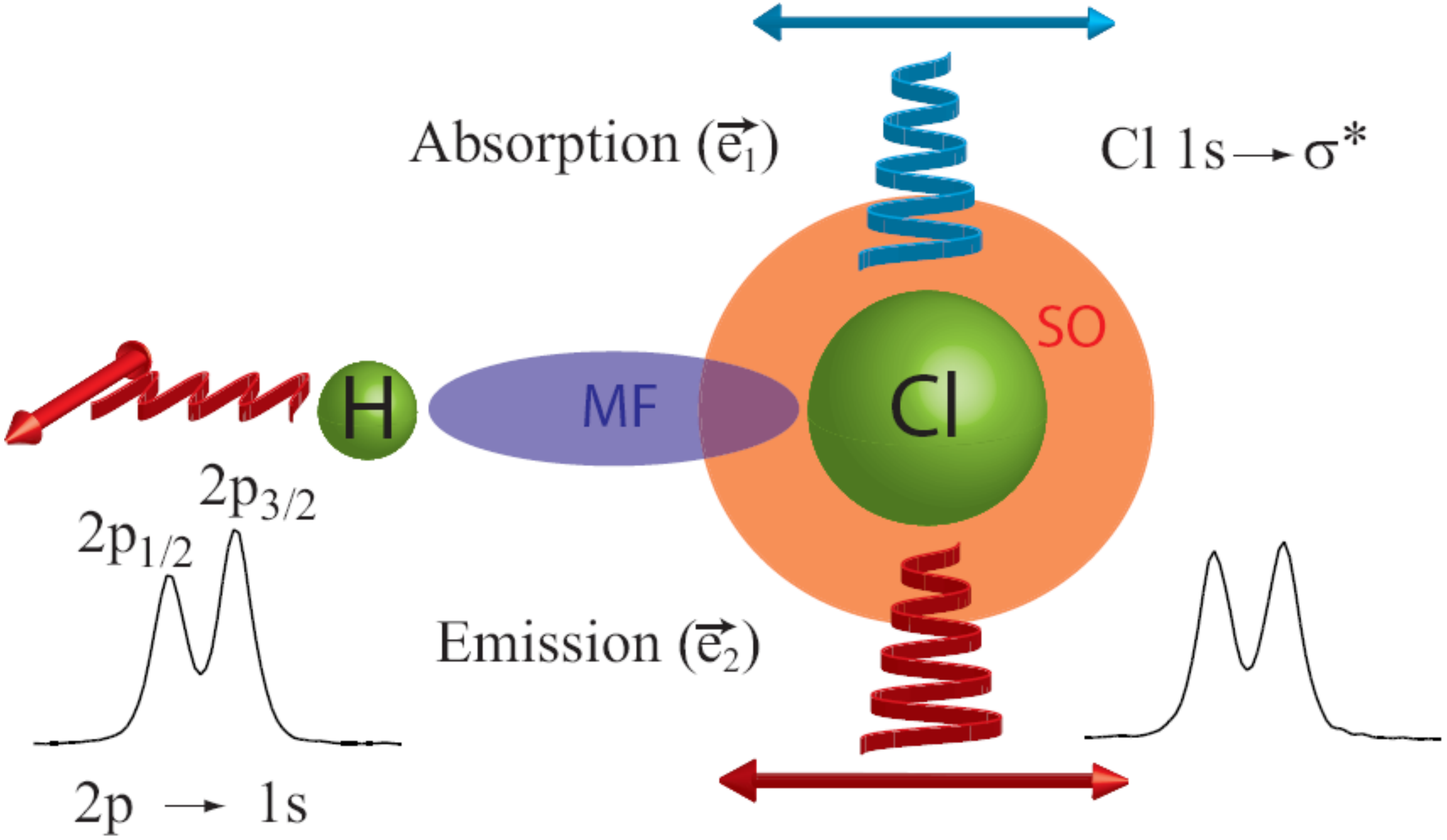

Polarised RIXS: influence of Molecular Field

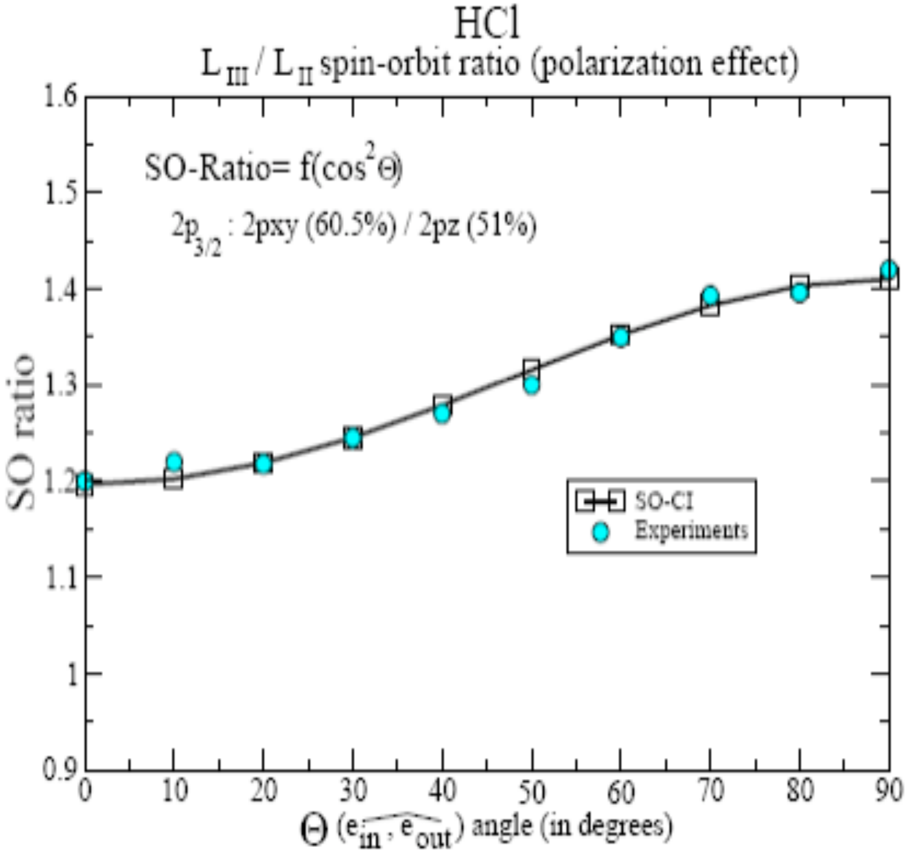

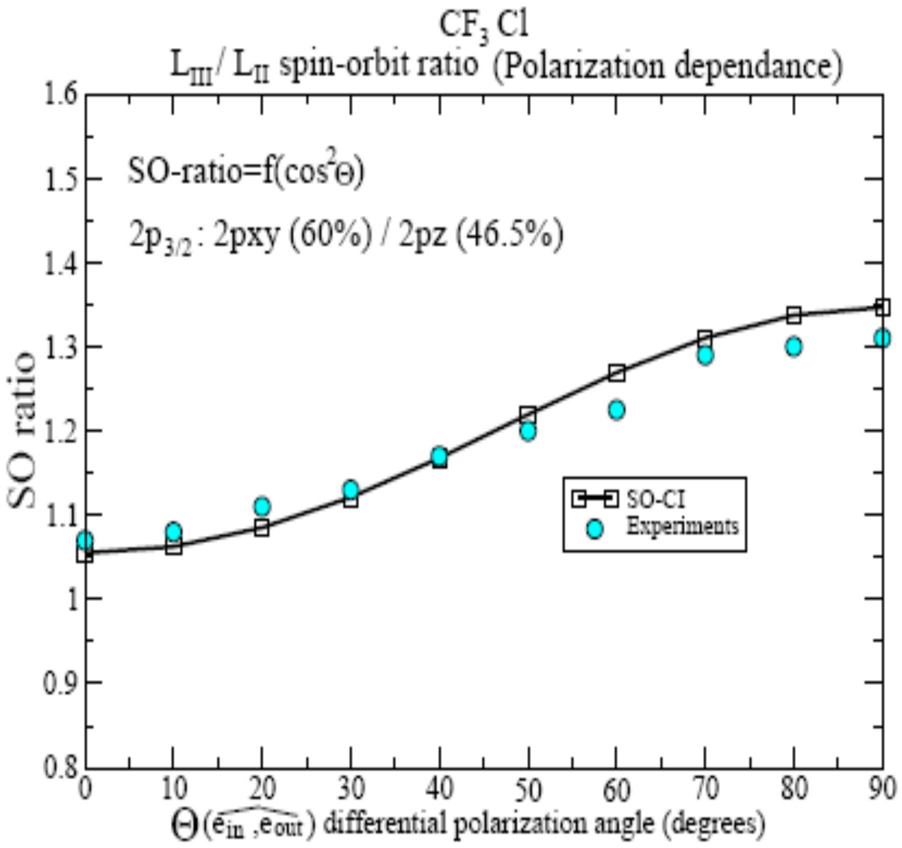

R. Guillemin, S. Carniato, W. C. Stolte, L. Journel, R. Taïeb, D. W. Lindle and M. Simon, Phys. Rev. Letters 101 133003 (2008)

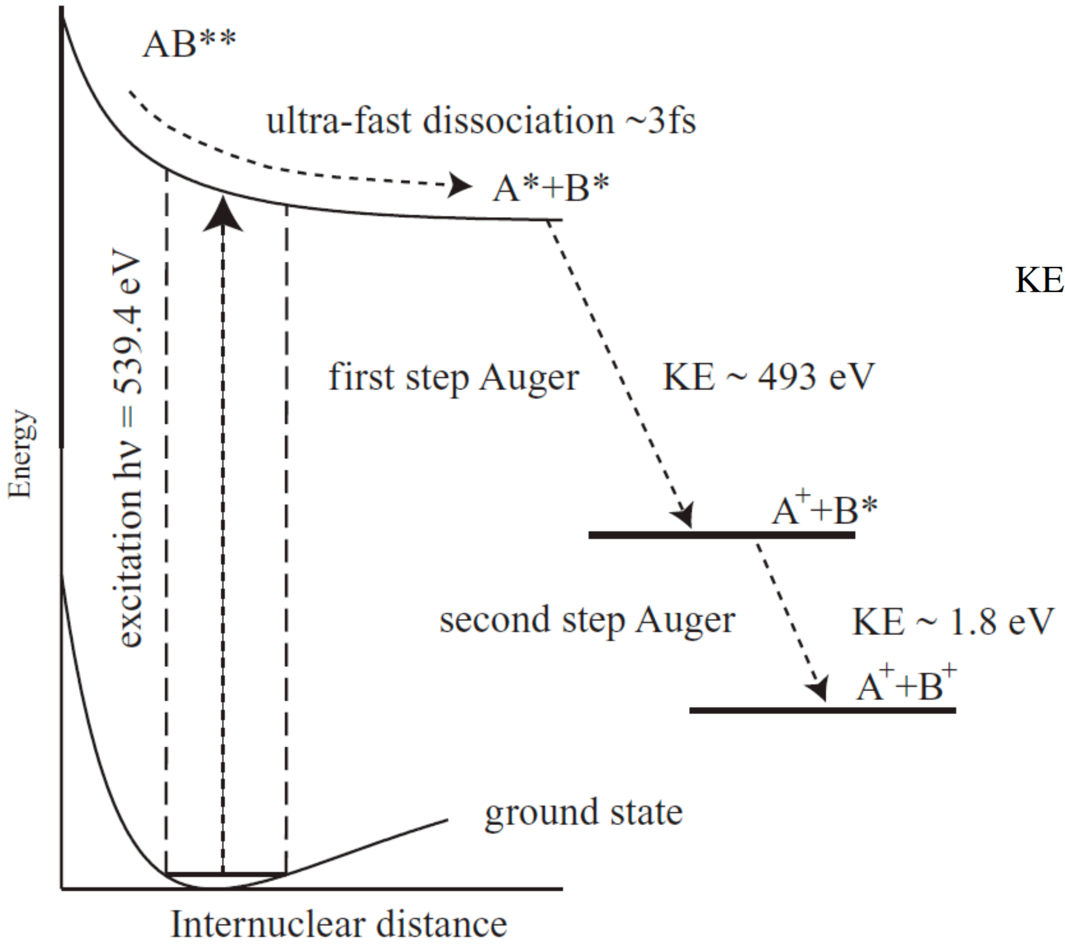

$$\mathrm{KER} = (3/32)\frac{m_A(1 + m_A/m_B)}{m_{\mathrm{elec}}}\frac{E_{\text{p-p}}^2}{E_{\mathrm{elec}}},$$

R. Guillemin, M. Simon and E. Shigemasa, **Phys. Rev. A 82** 051401 (2010)

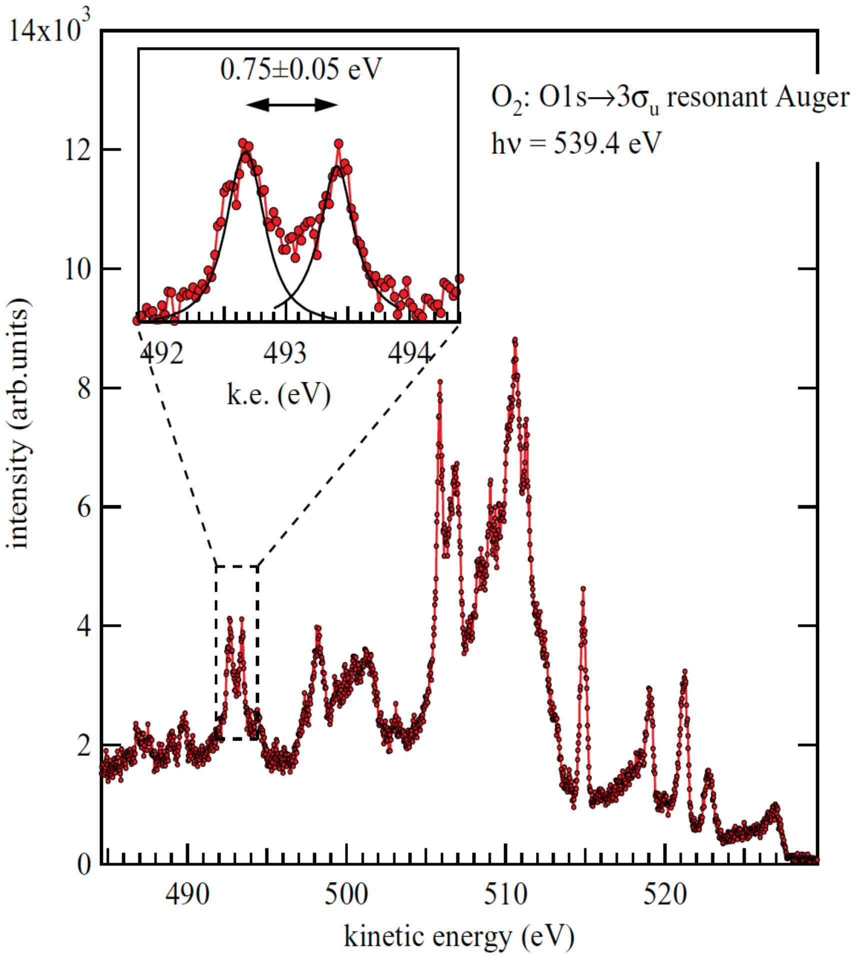

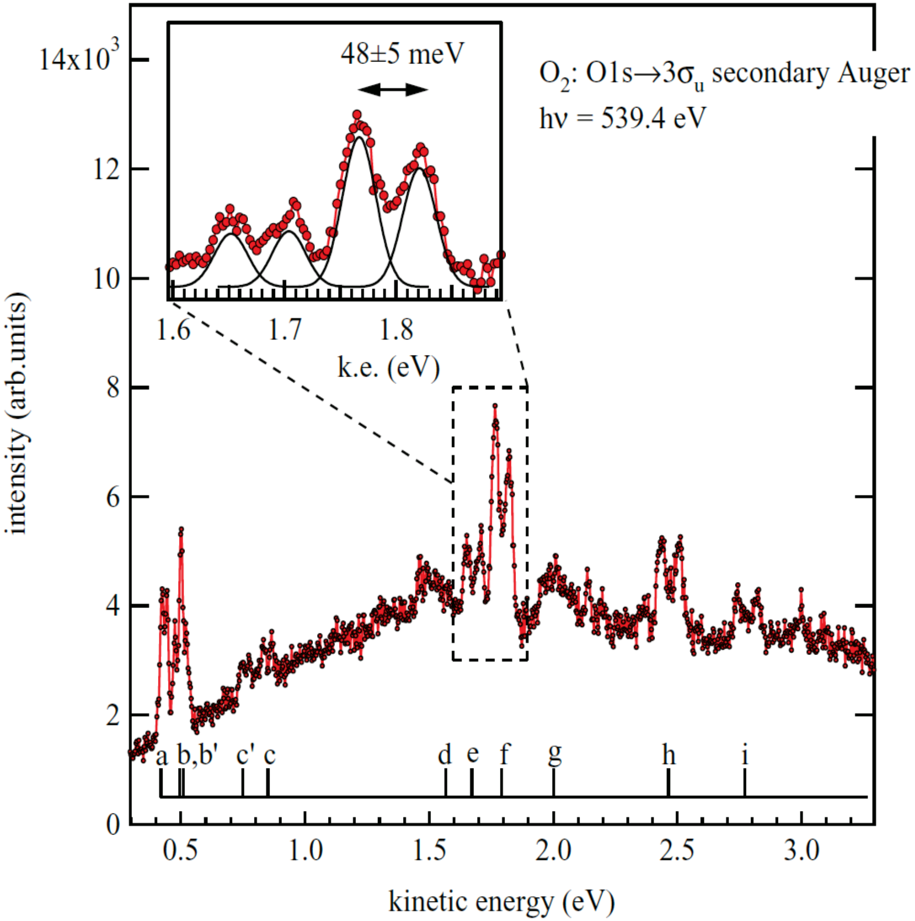

R. Guillemin, M. Simon and E. Shigemasa, **Phys. Rev. A 82** 051401 (2010)

Multiple ionization of Neon atoms

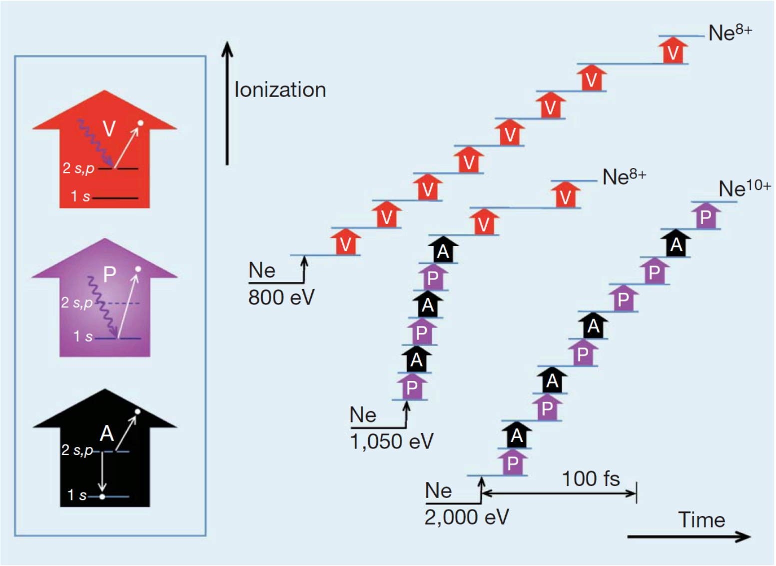

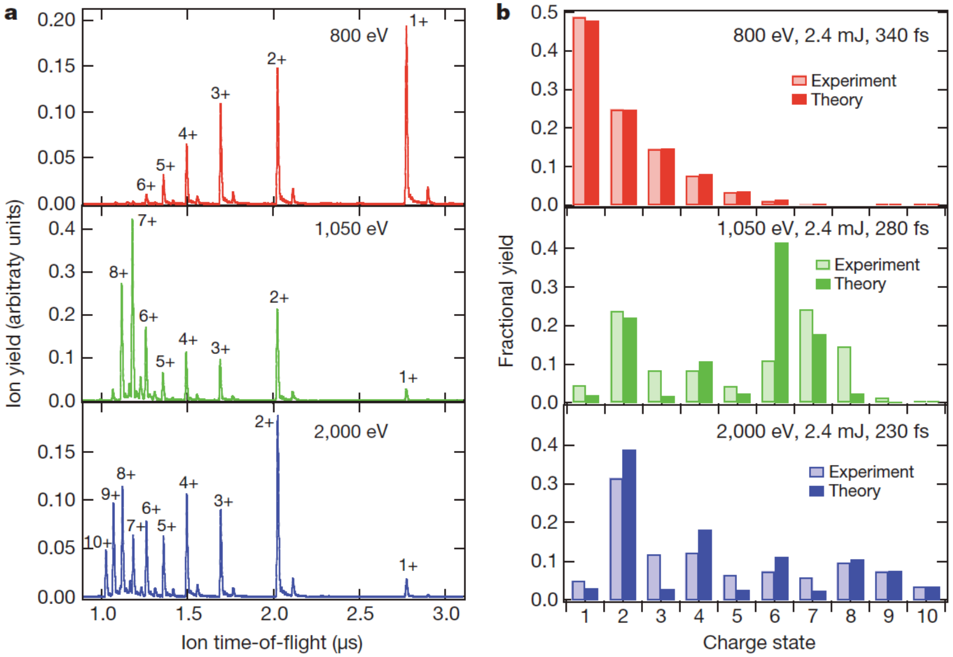

L. Young et al., Nature 466 (2010) 56